WHOLE SPACECRAFT VIBRATION ISOLATION SYSTEM: A COMPARISON OF PASSIVE VS. SEMI-ACTIVE VIBRATION ISOLATION DESIGNS

Behzad Jafari

A Thesis
in the Department
of
Mechanical and Industrial Engineering

Presented in Partial Fulfillment of the Requirements
for the Degree of Master of Applied Science (Mechanical Engineering) at
Concordia University
Montreal, Quebec, Canada

April 2018

Concordia University

School of graduate studies

This is to certify that the thesis prepared

By: Behzad Jafari

Entitled: Whole Spacecraft Vibration Isolation System: A Comparison of Passive vs. Semi-Active Vibration Isolation Designs

and submitted in partial fulfillment of the requirements for the degree of

Master of Applied Science (Mechanical Engineering)

complies with the regulations of the University and meets the accepted standards with respect to originality and quality

Signed by the final examining committee:

_____ Chair
TBA

_____ Examiner
Dr. Youmin Zhang, MIE

_____ Examiner
Dr. Wei-Ping Zhu, ECE
External to the Program

_____ Supervisor
Dr. Ramin Sedaghati, MIE

_____ Supervisor
Dr. Farhad Aghili, (Canadian Space Agency)

Approved by:

_____
Dr. S. Narayanswamy, M.A.Sc. Program Director
Department of Mechanical and Industrial Engineering

_____
Dr. Amir Asif, Dean
Faculty of Engineering & Computer Science

Date: April 11, 2018

Abstract

The launch phase is the harshest mechanical environment a spacecraft experiences through its lifetime. The severity of the vibrations during the launch phase poses a serious challenge for the design of the spacecraft which generally contains many sensitive electronic components. The need to guarantee the launch survival of the spacecraft has instigated a significant amount of research in the field of vibration isolation of the whole spacecraft, which resulted in development of various passive vibration isolation systems and their widespread use since two decades ago. The present study is aimed to analyze the feasibility of implementation of semi-active vibration isolation system instead of a passive one and to compare its potential benefits in attenuating the vibrations transmitted to the sensitive components of the spacecraft during the launch phase. First, the passive system has been studied and a methodology for design optimization of the multi-degree of freedom system in frequency and time domain has been formulated. The optimized passive system is then used as a baseline to compare the performance of the optimal passive isolator with that of a semi-active system. Semi-active control strategies based on Skyhook (SH) and combined Skyhook and Acceleration Driven Damping (SH-ADD) have been utilized to control the damping of the isolator between spacecraft and launch vehicle to attenuate vibration. The results showed that while semi-active system has a significant advantage over passive system to attenuate vibrations when the excitations are harmonic or narrow band, the results are not as promising when broadband random excitation, which is a realistic model of the excitations that the spacecraft experiences during launch, is considered. This calls into question the practical effectiveness of the semi-active system to be used in whole spacecraft vibration isolation system. Further research work with experimental tests are required to verify if semi-active systems can have a practical application in whole spacecraft isolation system.

Acknowledgment

First and foremost, I would like to appreciate my supervisors, Dr. Ramin Sedaghati and Dr. Farhad Aghili for their invaluable help and guidance through my entire Masters' and providing an enjoyable work environment.

I also like to express my gratitude to my partner, Melissa for providing me with unfailing encouragement and support, without which this work would not have been possible.

LIST OF FIGURES

NOMENCLATURE

ACRONYM	DESCRIPTION
LV	Launch Vehicle
SC	Spacecraft
SH	Skyhook
ADD	Acceleration Driven Damping
FRF	Frequency Response Function
PSD	Power Spectral Density
TF	Transfer Function
RMS	Root Mean Square
SDoF	Single Degree of Freedom
MDoF	Multi Degrees of Freedom

SYMBOL	DESCRIPTION
δ	Static deflection
ζ	Damping ratio
ω_n	Natural frequency
ϕ	Phase angle between deriving excitation and absolute displacement response
θ	Phase angle between deriving excitation and relative displacement response
m	Mass
k	Stiffness
c	Damping
$\boldsymbol{M}$	Mass matrix
$\boldsymbol{K}$	Stiffness matrix

$\boldsymbol{C}$	Damping matrix
$\boldsymbol{\psi}$	Matrix of mode shapes
$\boldsymbol{\Omega}$	Matrix of natural frequencies
$\{x\}$	Displacement vector in time domain
$\{\hat{X}\}$	Displacement vector in frequency domain
λ_r	Complex natural frequencies
$\boldsymbol{\theta}$	Matrix of complex mode shapes
$\{q\}$	Displacement vector in generalized coordinates
$\{\hat{Q}\}$	Frequency domain representation of displacement vector in generalized coordinates
$\boldsymbol{H_s}$	Matrix of frequency response functions in generalized coordinate
$\boldsymbol{H_p}$	Matrix of frequency response function in physical coordinate
c_{sa}	Semi-active damper
α	Cross-over frequency between SH and ADD control strategies

TABLE OF CONTENTS

CHAPTER1: Introduction, Literature Review and Objectives

1.1 Introduction

A spacecraft is subject to different dynamic mechanical loads during its lifetime, starting from its transportation, to its placement in the orbit and to its final disposal. The launch stage, which lasts only a few minutes, is the most severe stage during the life cycle of the satellite. Surviving the launch phase is the main consideration behind the structural design of satellites [1]. The severity of the launch stage has caused the designs of satellites to be very stiff or to locally isolate sensitive components. These methods, however, add weight to the spacecraft without any added functionality.

The *whole spacecraft vibration isolation system* is intended to add a soft connection between the spacecraft and the Launch Vehicle (LV) to reduce the load transferred to the whole spacecraft. Therefore, it adds reliability to the system while allowing for lighter components to be used on the spacecraft, and makes room for the weight of the payload to be used more efficiently.

The design and implementation of whole spacecraft vibration isolation is, however, challenging. This is mainly due to the severity of the launch environment and the complexity of the structures on both sides of the isolator. Since the isolator changes the dynamic response of the spacecraft, a full coupled load analysis is necessary. It should be guaranteed that there are no modes introduced with very low frequencies which can interfere with the altitude control system of the LV. There is also a limitation on the allowable relative displacement between the payload and the LV since the payload generally has a very limited space to move inside the fairing of the LV.

1.2 Literature review

1.2.1 Description of the mechanical loads during launch

During the launch spacecraft experiences the highest dynamic load[2]. The mechanical environment during launch is generally categorized as follows [3]:

1. **The quasi-static accelerations** generated by constant (or slowly changing) external forces. These forces include gravity, the thrust of the engine(s), and the drag force. Since these forces are static or quasi-static, they do not generate a significant dynamic response in the spacecraft.
2. **The low frequency dynamic response** occurs because of interaction between the LV/payload modes. These loads are typically considered to have a frequency range from 5-100Hz, depending on the type of structure.
3. **High frequency random vibration** having significant energy in the 20-2000Hz frequency range. Acoustic loads which include the noise of the launch vehicle engines, the separation of the airflow along the launch vehicle, and the aerodynamic noise, is the main source of these loads.
4. **Pyrotechnic shock loads** with an energy spectrum measured at 100-10000Hz.

The primary objective of the whole spacecraft vibration isolation system is to attenuate the low frequency dynamic response for the primary structures. However, it also has a positive effect in reducing the load transmitted to the satellite during the high frequency random vibrations and shock events, which is the secondary goal of the isolation system.

1.2.2 Passive whole spacecraft vibration isolation

The practical implementation of a whole spacecraft vibration isolation system has been studied since 1993 [4]. The major problem was that the GFO (a US navy earth observation satellite) had an unacceptably low stress margin around the resonant burn[1] frequency of the solid rocket motor Castor 120, which is around 45-60Hz. Therefore, the need arose to reduce the dynamic response of the payload around that frequency range, which became the primary goal. The secondary goal was the reduction of loads transferred to the satellite at other frequencies while guaranteeing low relative displacement between the satellite and the fairing. The result was the Soft Ride system, which had its first successful launch with Orbital's Taurus launch vehicle in 1998. Since then, the whole spacecraft vibration isolation system has been used many times for different launches**.** Some LV providers, such as Taurus and Minotaur, are already providing the payload isolation system as an optional service.

Since the successful launch of satellites with passive isolation systems, more researchers have taken an interest in the field of passive vibration isolation of a whole spacecraft. There have been significant developments in the practical design and testing of new passive isolator ideas [5, 6] as well as theoretical developments, in particular in the field of coupled load analysis (CLA) [7-9] which is the most challenging part of the design of an isolation system[10].

[1] Resonant burn is a phenomena observed in solid fueled rockets with cavity. It happens when the pressure oscillations couples with the natural frequency of the combustion cavity and can cause significant vibration in the system.

1.2.3 Shortcomings of passive vibration isolation systems

Despite the advantages that passive vibration isolation of a whole spacecraft system offers, there are some fundamental limitations inherent to any passive vibration isolator. These limitations are:

1. Higher vibration attenuation requires larger static deflection of the isolator which may interfere with the available space.
2. Effective for narrow band frequency ranges due to lack of adaptability. High damping is desirable for low frequency region (specially near the resonance frequency) while increasing damping increases the vibration transmission at higher frequencies.
3. The contradictory behavior between the relative displacement and the absolute acceleration of the isolated mass. This means that any attempts to reduce the acceleration of the isolated mass should take into account the relative displacement and available stroke.

To fundamentally investigate these limitations, here the steady state behavior of a viscously damped single degree of freedom system subject to harmonic base excitation as shown in Figure 0.1.is analyzed.

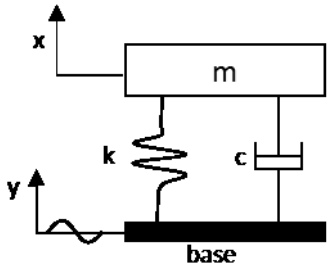

Figure 0.1: Passively isolated SDoF system subject to base excitation

The static deflection, δ, for the system, can be evaluated as:

$$k\delta = mg \rightarrow \delta = \frac{mg}{k} = \frac{g}{\omega_n^2} \tag{0-1}$$

where ω_n ($\omega_n = \sqrt{\frac{k}{m}}$) is the undamped natural frequency of the system. Eq. (*0-1*) shows that the static deflection is inversely proportional to the square root of the natural frequency of the system. To reduce the vibration transmitted from the base to the isolated mass, the isolator's natural frequency should be as low as possible. This is due to the fact that the attenuation starts from frequencies above $\sqrt{2}\omega_n$. Therefore, the lower the natural frequency, the wider the range of the frequencies that the isolator can attenuate, thus having better performance, however low isolation frequency will cause larger static deflection as given in Eq. (1-1) which may interfere with available space. It is also important to note that for a Launch Vehicle/ Spacecraft (LV/SC) system, in addition to 1g (the weight of the payload) the SC generally goes through additional quasi-static acceleration which can go up to about 6g in the axial direction due to the thrust of the motor(s) [11]. This means that the static deflection can become a significant limitation for the design of passive whole spacecraft vibration isolation system.

The second limitation addressing inability of passive isolators to provide different damping levels; is well-known and mentioned in many texts on vibration. To examine this, let us write the governing equation of motion for the SDoF system shown in Figure 0.1 as

$$m\ddot{x} + c(\dot{x} - \dot{y}) + k(x - y) = 0 \tag{0-2}$$

or, dividing the equation by mass m, as

$$\ddot{x} + 2\zeta\omega_n(\dot{x} - \dot{y}) + \omega_n^2(x - y) = 0 \tag{0-3}$$

where ζ is the damping ratio ($\zeta = \frac{c}{2\sqrt{mk}}$). Now consider the base motion, y to be harmonic with an amplitude of Y, represented as

$$y = Y\sin(\omega t) \tag{0-4}$$

Then, since the system is linear, the steady state part of the solution contains the same frequency as the excitation frequency with difference only in the phase and amplitude. That is to say the particular, or steady state, solution is expressed as

$$x_p = X\sin(\omega t - \phi) \tag{0-5}$$

where $\phi = \tan^{-1}\left(\frac{2\zeta r^3}{1+r^2(1-4\zeta^2)}\right)$ is the phase angle, representing the phase difference between the excitation and the response, and X is the displacement amplitude of the steady state oscillation of the isolated mass which can be expressed as

$$\frac{X}{Y} = \frac{\sqrt{1 + (2\zeta r)^2}}{\sqrt{(1 - r^2)^2 + (2\zeta r)^2}} = \frac{\ddot{X}}{\ddot{Y}} \tag{0-6}$$

in which $r = \frac{\omega}{\omega_n}$ represents the normalized excitation frequency.

Figure 0.2 shows the results for the normalized absolute amplitude of the response with respect to the normalized frequency for different values of damping ratio, ζ. It is noted that since the

response is harmonic, the ratio of displacement amplitude is equivalent to the acceleration amplitude ($\frac{X}{Y} = \frac{\omega^2 X}{\omega^2 Y} = \frac{\ddot{X}}{\ddot{Y}}$).

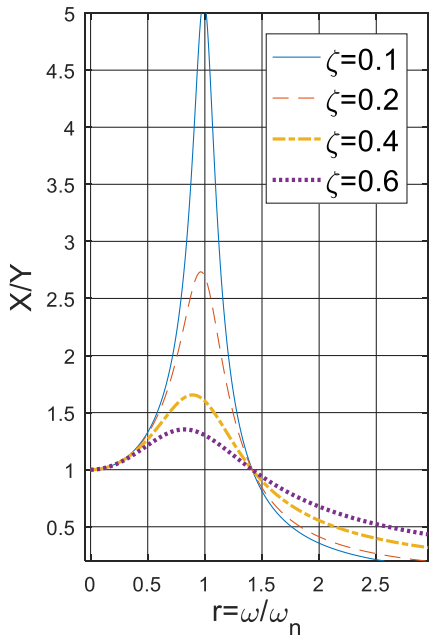

Figure 0.2: Frequency response of isolated mass displacement (acceleration) for an SDoF system

The trade-off between the amplification of the response at resonant frequency and the attenuation of the response at higher frequencies can be readily seen in Figure 0.2. It should also be noted that above frequency $\sqrt{2}\omega_n$, increasing damping yields higher response as discussed before.

To address the third limitation of passive systems mentioned before, let us write the equation of motion, now in terms of relative displacement $z = x - y$, as

$$\ddot{z} + 2\zeta\omega_n\dot{z} + \omega_n^2 z = -\ddot{y} = \omega^2 Y \sin\omega t \qquad (0\text{-}7)$$

The particular (or steady-state) response for the relative displacement between the base and the isolated mass is represented as

$$z_p = Z\sin(\omega t - \theta) \tag{0-8}$$

where $\theta = \tan^{-1}\left(\frac{2\zeta r}{1-r^2}\right)$ is the phase angle between the deriving excitation and relative displacement. The amplitude of the steady sate relative displacement, Z over the amplitude of the base displacement, Y, can be expressed as

$$\frac{Z}{Y} = \frac{r^2}{\sqrt{(1-r^2)^2 + (2\zeta r)^2}} \tag{0-9}$$

Now considering Eqs. (1-6) and (1-9), the ratio of amplitude of steady state acceleration of the sprung mass, $\ddot{X}$ over the amplitude of the steady state relative displacement, Z can be expressed as

$$\lambda = \left|\frac{\ddot{X}}{Z}\right| = \frac{\omega^2 X}{Z} = \omega^2\left[\frac{\sqrt{1+(2\zeta r)^2}}{r^2}\right] = \omega_n\sqrt{\omega_n^2 + (2\zeta\omega)^2} \tag{0-10}$$

It is clear from Eq. ((0-10) that the ratio $\left|\frac{\ddot{X}}{Z}\right|$ monotonically increases as a function of natural frequency, ω_n and the damping ratio ζ, at any excitation frequency, ω.

Let us consider the case in which the magnitude of the steady state acceleration, $\ddot{X}$, is required to be constant ($\ddot{X} = C_1$), thus we can write

$$\lambda = \frac{\ddot{X}}{Z} = \frac{C_1}{Z} = \omega_n\sqrt{\omega_n^2 + (2\zeta\omega)^2} \rightarrow Z = \frac{C_1}{\omega_n\sqrt{\omega_n^2 + (2\zeta\omega)^2}} \tag{0-11}$$

Eq. ((0-11) states that the amplitude of the steady state relative displacement, Z *decreases* with the increase of ω_n or ζ at any excitation frequency ω. Now when Z is assume to be constant ($Z = C_2$), we have

$$\lambda = \frac{\ddot{X}}{C_2} = \frac{\ddot{X}}{C_2} = \omega_n\sqrt{\omega_n^2 + (2\zeta\omega)^2} \rightarrow \ddot{X} = C_2\omega_n\sqrt{\omega_n^2 + (2\zeta\omega)^2} \qquad (0\text{-}12)$$

Eq. ((0-12) shows that $\ddot{X}$ behaves exactly opposite to Z. That is to say that the amplitude of steady state absolute acceleration of the isolated mass, $\ddot{X}$ *increases* as either ω_n or ζ increase, at any excitation frequency. This observation is also shown in [12], where an optimization is conducted for steady state response of the system for different choices of objective function.

Another problem regarding the practical implementation of a passive vibration isolation system is that compliance in one axis often results in compliance in another axis. Therefore, it is generally not possible to control the stiffness in different axes independently [11].

To alleviate these shortcomings of the passive systems, active isolators, shown schematically in Figure 0.3, can be used. In [11], an active isolation system for payload is designed and tested. The results show that by using a hybrid (active-passive) system, the resonant peak can be reduced without deteriorating the isolation performance at higher frequencies. The same article, however, suggests semi-active isolator design to be developed for future works as it can have a performance similar to the active design without many of its drawbacks.

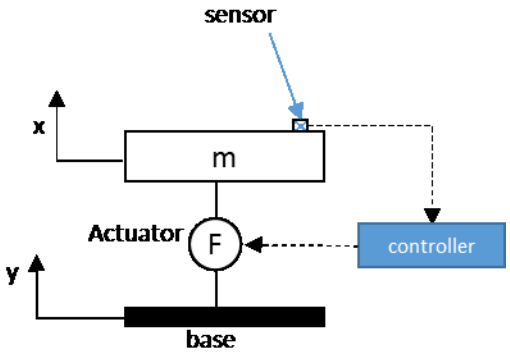

Figure 0.3: Schematic representation of active vibration isolation system

The drawbacks of the active system are increased cost, complexity, and weight to the system. Active isolation systems are also subject to problems such as the possibility of destabilizing the system since the isolator is adding energy to the system, and the total loss of isolation performance in case of failure of the control (in other words, they are not fail-safe).

Semi-active vibration isolators, shown schematically in Figure 0.4, are filling the gap between passive and active isolation systems. They are less complex, lighter, and less costly than active isolation systems while having a performance close to active isolators [13]. In the case of failure of the control, they act as a passive isolator (they are fail-safe). And since they do not add any energy to the system, but rather just dissipate energy at a variable rate, they cannot cause destabilization of the system.

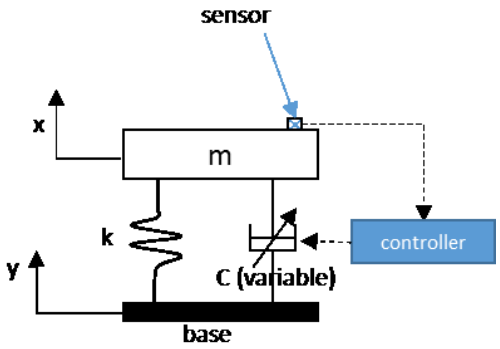

Figure 0.4: Schematic representation of semi-active vibration isolation system

1.2.4 Semi-active and active isolation systems for whole spacecraft vibration isolation

Following the successful design and widespread use of semi-active dampers in other applications including car suspension systems, the idea of using semi-active dampers in whole spacecraft vibration isolation has been developed [15].

In [16, 17], a semi-active system based on variable damping using MR dampers, is designed and tested with a single degree of freedom payload, in axial direction. The results showed substantial improvement of the isolation performance when a semi-active damper is used instead of a passive one. The limitation of that work is that the design and test is carried out for an SDoF payoad in a single axial direction, and the flexibility of both LV and satellite are not taken into consideration.

1.2.5 Modeling of the system

When modeling the LV/SC system, it should be noted that both structures are flexible with many natural frequencies and mode shapes in the axial as well as in the lateral direction, although higher modes may not be considerably excited.

One of the main objectives of the present study is to develop a design optimization methodology for an MDoF system representing launch vehicle (LV) stages, payload and subcomponents (constituting the model of the satellite) subjected to base harmonic and impulse excitations. The lumped masses (subcomponent, payload and LV stages) are connected to one another via an isolation system. The challenge is that there is no control over the mechanical characteristics of either side of the connection, both the LV and the satellite, which are generally provided by different companies, each have dynamic characteristics which are generally not subject to variation unless they are being re-designed, which is a costly and time-consuming process. Only the dynamic characteristics of the isolation system (stiffness and damping) can adjusted to attenuate vibration transmission to sensitive components. This concept is shown schematically in **Error! Reference source not found.**, where a typical global damping or stiffness matrix is shown for a whole spacecraft vibration isolation system.

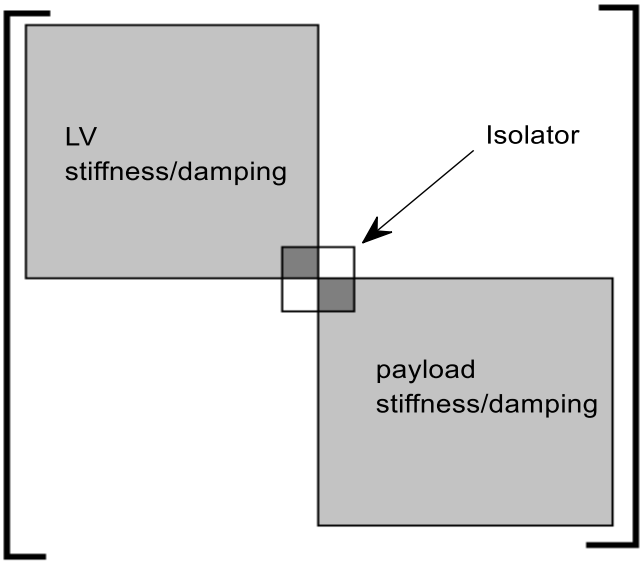

Figure 0.5: General form of stiffness/damping matrix for LV/payload passive isolator

In recent years there have been several attempts to derive a method to analytically measure the isolation performance between a pair of flexible structures. Zheng [18] considers the above-mentioned problem and develops analytical formulation to address the coupling between multi-stage launch vehicle and satellite for the case where the system is undamped. It is noted that the modal matrix will be real when the system is undamped or proportionally damped (proportional and un-proportional damping is discussed in Chapter 2). Here, in the present work, the case where the damping is not proportional and therefore the modal matrix is complex has been investigated.

For the complete design of the whole spacecraft vibration isolation system, a full finite element model of the LV and the payload (satellite) and other subcomponents is generally needed. However, in the preliminary stages of design the system can be reduced to few degrees of freedom using lumped mass approaches to demonstrate the effect of isolator parameters on response of the system as well as the performance analysis and comparison of different control strategies when a semi-active isolator is used instead of a passive one.

In the present thesis, similar to [19], [20] and [8], a benchmark four DoF lumped mass system representing the coupling between the LV and the spacecraft as shown in **Error! Reference source not found.** has been considered

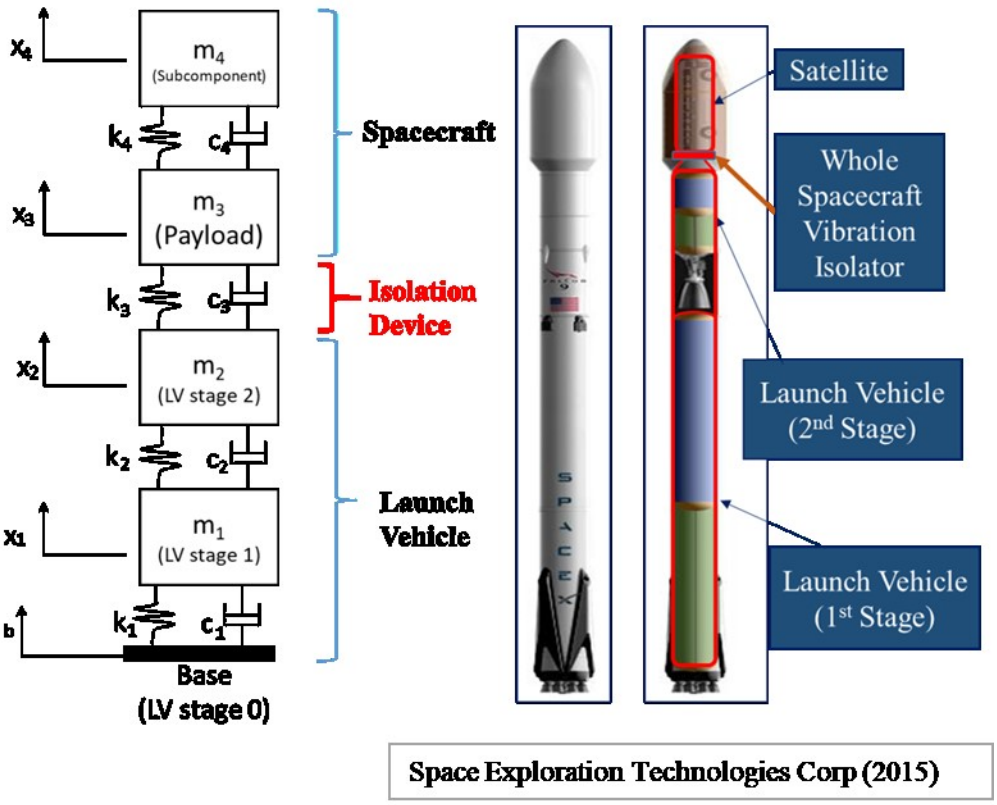

Figure 0.6: Simplified model of the LV/spacecraft

The launch vehicle is assumed to be consist of three stages. However, since the mass of the first stage is considerably more than the other stages of the LV, it is assumed to be the "base". Using Newton's second law and free body diagram for each component, governing equations of the motion of the system can be derived and then cast into the matrix format as

$$\begin{bmatrix} m_1 & & & \\ & m_2 & & \\ & & m_3 & \\ & & & m_4 \end{bmatrix} \begin{Bmatrix} \ddot{x}_1 \\ \ddot{x}_2 \\ \ddot{x}_3 \\ \ddot{x}_4 \end{Bmatrix} + \begin{bmatrix} c_1 + c_2 & -c_2 & & \\ -c_2 & c_2 + c_3 & -c_4 & \\ & -c_3 & c_3 + c_4 & -c_4 \\ & & -c_4 & c_4 \end{bmatrix} \begin{Bmatrix} \dot{x}_1 \\ \dot{x}_2 \\ \dot{x}_3 \\ \dot{x}_4 \end{Bmatrix}$$
$$+ \begin{bmatrix} k_1 + k_2 & -k_2 & & \\ -k_2 & k_2 + k_3 & -k_3 & \\ & -k_3 & k_3 + k_4 & -k_4 \\ & & -k_4 & k_4 \end{bmatrix} \begin{Bmatrix} x_1 \\ x_2 \\ x_3 \\ x_4 \end{Bmatrix} = \begin{Bmatrix} c_1\dot{y} + k_1 y \\ 0 \\ 0 \\ 0 \end{Bmatrix} \tag{0-13}$$

In Eq. (0-13), as discussed before, the only design parameters prone to variation are the isolator's dynamic parameters (stiffness, k_3 and damping constant, c_3). Other stiffness and damping constants are pre-determined by the structure of the LV and SC as mentioned before. The effect of these design parameters on the system stiffness and damping matrices is clearly shown in **Error! Reference source not found.**.

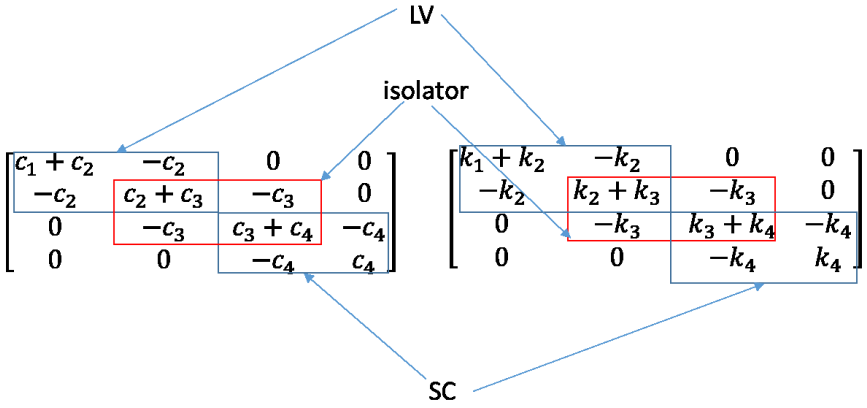

Figure 0.7: General form of stiffness/damping matrix for LV/payload passive isolator

1.2.6 Time and frequency analysis

The main concern in the present study is the damage and failure of sensitive components of the payload. Failure may occur by excessive force transmitted during transient events, by instability during a particular operation condition, or by fatigue [21]. The design of the isolation system needs to guarantee against all types of failure.

To design against excessive force first the magnitude of peak force transmitted to the payload needs to be determined, which is proportional to the absolute acceleration of the isolated mass. When the system is excited, the maximum acceleration of the isolated mass happens at the first

few oscillations of the isolated mass, before the transient part of the response damps out. Therefore, the analysis of the system should take the transient part of the response into account to find the maximum response of the system. It should be noted that using classical frequency analysis does not provide such information. Therefore, the analysis should be done in the time domain.

To design against fatigue failure, the steady state solution is of more importance than the transient solution. The reason for this is that the transient solution, although important in determining the peak of the response, dies out quickly as a result of damping. Thus, its contribution is not major in fatigue failure of the components. The steady state solution can be analyzed by transferring the governing equations of the system to frequency domain using Fourier transform and deriving the frequency response function (FRF) of the system.

A frequency analysis can also provide the information needed to guarantee the stability of the system in the frequency range of interest. For example, for a LV/SC system it is necessary to guarantee that the system does not have very low frequency modes with high amplitude as they may interfere with altitude control system of the LV. Another concern is around the resonant burn frequency where the system undergoes significant excitation. The isolation design needs to guarantee that the response of the system is stable under these conditions. In the present study, an analysis of both time and frequency domains have been performed on the system.

1.2.6 Performance indices

Because in the present thesis both linear passive systems and nonlinear semi-active systems will be analyzed and compared, it is necessary to use approprate performance indices that is aplicable to both these systems for fair comparision. The performance indices will also be used as

objective functions in the design optimization formulation to optimize the design variables for the isolation system in both time and frequnecy domains.

Since the main objective is to protect sensitive payload equipment from base excitation, the primary goal would be to reduce the absolute acceleration of the isolated mass while there is limitation on the relative displacement between the payload and the launch vehicle due to the available stroke.

For linear systems, valuable information can be obtained with regard to system performance by taking the Fourier transform of the equations of motion of the system and finding the transfer function (TF) and frequency response function (FRF) of the system. The significance of TF and FRF lies in the fact that for a linear system, the steady state response of the system contains only the same frequencies as the driving frequency, with difference only in phase and amplitude. This is, however, not the case for nonlinear systems. Therefore, the concepts of FRF and TF are not restrictedly applicable to a semi-active system which is highly nonlinear.

An equivalent frequency response (approximate FRF) for nonlinear semi-active systems can be used based on the concept of variance gain. This concept is used in the design of semi-active (nonlinear) car suspension systems [12]. The variance gain can be decribed as

$$\hat{F}_{acc} = \sqrt{\frac{\frac{1}{T}\int_0^T (x(t))^2 dt}{\frac{1}{T}\int_0^T (u(t))^2 dt}} \tag{0-14}$$

where $u(t)$ represents the input signal and $x(t)$ is the output signal. This is equal to the RMS value of the output signal over the input signal.

For nonlinear systems, the approximate variance gain can be calculated by subjecting the system to different tonal vibration ($u_i = \sin(\omega_i t)$) and taking the RMS of the steady state response of the output signal (the acceleration of the isolated mass in this case) at discrete frequnecies divided by the RMS of the input signal. It should also be noted that since the input signal is a harmonic with amplitude *A*, the RMS value will always be equal to $\frac{A\sqrt{2}}{2} = 0.707A$, given that the signal is taken over a long enough duration. Then, the variance gain can be calculated as [12]

$$\hat{F}_{acc} = \sqrt{\frac{\frac{1}{T}\int_0^T (x_i(t))^2 dt}{\frac{1}{T}\int_0^T (u_i(t))^2 dt}} = \frac{RMS(x_i(t))}{RMS(u_i(t))} \qquad for\ i = 1,2,\dots,N \tag{0-15}$$

It should noted that for linear systems, Eq. (0-15) simply becomes the magnitude of the transfer function of the system. However, in order to gurantee that the result of Eq. ((0-15) (that is to say the RMS ratio of output over input) is accurate and represents the frequncy response function of the system, it is neccesary to first allow the transient part of the rsponse to damp out since the transient portion of the response of the system contains frequencies that are different from excitation frequency (even when the system is linear) and therefor considering them will reduce the accuracy of the results.

The RMS value of a signal can also be calculated in frequency domain, using Parseval's theorem. Parseval's theorem states that the sum of the squares of a function in the time domain equals the sum of the squares in the frequency domain. In other words, the theorem states that the total energy of a signal in time domain is equal to that in frequency domain, which is expressed as

$$\int_{-\infty}^{\infty} x(t)^2 dt = \frac{1}{2\pi}\int_{-\infty}^{\infty} \hat{X}(\omega)^2 d\omega \tag{0-16}$$

where $\hat{X}(\omega)$ represents the Fourier transform of the time domain signal $x(t)$.

Therefore, the RMS of a signal, *X*, within a certain frequency range $[\omega_i - \omega_f]$ can be defined as [12]:

$$RMS(X) = \sqrt{\frac{1}{\omega_f - \omega_i}\int_{\omega_i}^{\omega_f} X(\omega)^2 d\omega} \tag{0-17}$$

Using Eq. (1-17), the perfomance index or objective function for the optimization problem in the frequency domain may be written as

$$\hat{F}_{acc} = \frac{RMS(X)}{RMS(U)} = \sqrt{\frac{\int_{\omega_i}^{\omega_f} X(\omega)^2 d\omega}{\int_{\omega_i}^{\omega_f} U(\omega)^2 d\omega}} \tag{0-18}$$

For the time domain optimization, the maximum of the output over the maximum of the input signal should be used as the performance index (peak to peak ratio in time domain). The transient effect is also taken into accout. This may be represented as

$$F_t = \frac{MAX(|x_i(t)|)}{MAX(|u_i(t)|)} \qquad for\ i = 1,2,\dots,N \tag{0-19}$$

In the present thesis, optimization based on both time and frequency has been carried out and the results are compared.

Finally to compare the response of the system to random excitation the Power Spectral Density (PSD) of the signal is used. The PSD of a signal is a measure of the energy that a signal contains at different frequencies and is typically used to compare the random vibration data.

1.3 Objectives and Motivation

In the past two decades a significant amount of work has been devoted to the problem of vibration isolation between a pair of flexible structures using passive, semi-active, and active isolator designs. The issue has been extensively researched and documented in the literature. However, despite the design and test of semi-active or active systems, these systems have not been thoroughly studied for whole spacecraft isolation.

This thesis presents the analysis and optimization procedure of a passive isolator, and then compares the best results which can be achieved by a passive isolator with a semi-active isolation system. Vibration isolation between a pair of flexible structures using passive isolator and semi-active isolator with variable damper using different control strategies is analyzed and the results are compared.

1.4 The organization of the thesis

Chapter 1 presents the relevant literature and some fundamental concepts as well as the objective of the thesis. Chapter 2 starts with a simplified model of the LV-payload provided in Chapter 1 with the goal of achieving an optimized design of passive vibration isolator for a whole spacecraft. The optimization problems for a vibration isolation system between a pair of flexible structures in time and frequency domain have been formulated and the limitations of the passive isolation system are shown. The optimized passive system is then used as the base-line to compare the performance of semi-active vibration isolation designs. In Chapter 3 a semi-active isolator is designed and different control strategies are then compared. In Chapter 4 the results from different isolation systems are compared and the contributions and the limitations of these

findings are discussed, and future research on the topic of vibration isolation of the whole spacecraft is recommended.

CHAPTER 2: Analysis and Optimization of Passive Isolation System

2.1 Introduction

As discussed before, the inherent contradiction of the passive isolator limits its performance in wide range of frequencies. It should be noted, however, that despite its limitations, the reliability, simplicity and low cost of passive isolators have made them the most common method of vibration isolation in industry, particularly when the goal of isolation is protection of the payload from a harsh mechanical environment.

In this section, the model described in section 1.2.5 to represent the LV/Spacecraft is considered as the benchmark for further development. First modal analysis has been conducted to investigate the effect of variation of isolator parameters (damping and stiffness constants) on all the modes of the system. Then a design optimization problem has been formulated to identify the optimum parameters of the passive isolator that minimizes the absolute acceleration of the payload while guaranteeing minimum relative displacement between the payload and the LV. The optimization is first conducted in frequency domain and then in time domain. The results obtained from this chapter, is used as a baseline to compare the performance of different semi-active systems in the fallowing chapter.

2.2 Derivation of FRF and modal analysis

Here the model of the LV/spacecraft and its equations of motion are reproduced from Chapter 1 for the sake of clarity.

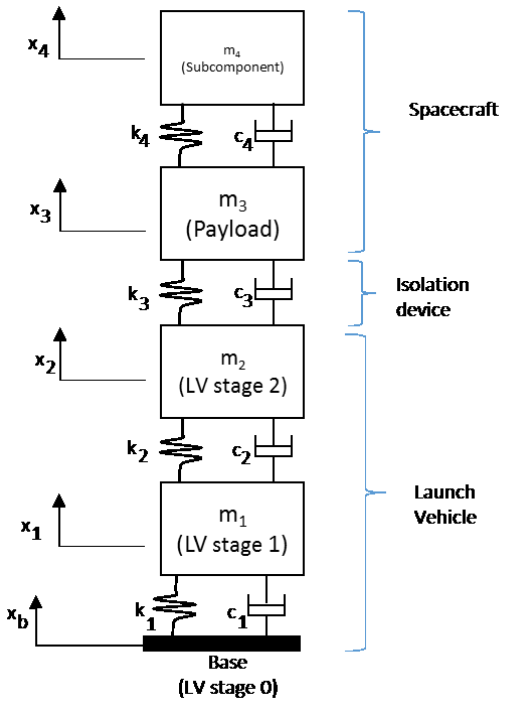

Figure 2.1Figure 0.6: Simplified model of the LV/spacecraft

$$\begin{bmatrix} m_1 & & & \\ & m_2 & & \\ & & m_3 & \\ & & & m_4 \end{bmatrix} \begin{Bmatrix} \ddot{x}_1 \\ \ddot{x}_2 \\ \ddot{x}_3 \\ \ddot{x}_4 \end{Bmatrix} + \begin{bmatrix} c_1 + c_2 & -c_2 & & \\ -c_2 & c_2 + c_3 & -c_4 & \\ & -c_3 & c_3 + c_4 & -c_4 \\ & & -c_4 & c_4 \end{bmatrix} \begin{Bmatrix} \dot{x}_1 \\ \dot{x}_2 \\ \dot{x}_3 \\ \dot{x}_4 \end{Bmatrix} + \begin{bmatrix} k_1 + k_2 & -k_2 & & \\ -k_2 & k_2 + k_3 & -k_3 & \\ & -k_3 & k_3 + k_4 & -k_4 \\ & & -k_4 & k_4 \end{bmatrix} \begin{Bmatrix} x_1 \\ x_2 \\ x_3 \\ x_4 \end{Bmatrix} = \begin{Bmatrix} c_1\dot{x}_b + k_1 x_b \\ 0 \\ 0 \\ 0 \end{Bmatrix} \quad ((0\text{-}13)$$

In order to conduct the optimization, it is required to obtain FRF relating the acceleration of the subcomponent to the input acceleration at the base.

Here first eigenvalues (frequencies) and the corresponding eigenvectors (mode shapes) of the system have been identified using free vibration analysis. The governing equation for the free vibration can be stated in matrix form as

$$[\boldsymbol{K} - \boldsymbol{\Omega^2 M}]\boldsymbol{\psi} = \vec{0} \tag{0-2}$$

in which diagonal matrix ($\boldsymbol{\Omega^2} = \left[\nwarrow\ \omega_{n,i}^2\ \searrow\right]$) contains the squared of natural frequencies and each column of the mode shape matrix ($\boldsymbol{\psi}$) represents the associated mode shapes.

Transforming equations of motion, Eq. (2-1) to the frequency domain, one can write:

$$\vec{\hat{X}}[-\omega^2\boldsymbol{M} + \omega j\boldsymbol{C} + \boldsymbol{K}] = \vec{\hat{f}}(\omega) \tag{0-3}$$

where $\vec{\hat{f}} = (c_1 j\omega + k_1)\hat{X}_b$. Then introducing the transfer function as

$$\boldsymbol{H}(j\omega) = [-\omega^2\boldsymbol{M} + \omega j\boldsymbol{C} + \boldsymbol{K}]^{-1} \tag{0-1}$$

we can write the output resposne in frequnecy domain as:

$$\vec{\hat{X}} = \boldsymbol{H}(j\omega)\ \vec{\hat{f}}(j\omega) \tag{0-2}$$

where the frequency response function, $\boldsymbol{H}$, here relates the displacement vector in frequency domain to the forcing function. The direct approach is, however, an inefficient method for system, with many DoFs as the determination of the response of the system at each frequency, requires evaluation of a matrix inverse of $n \times n$ matrix. Although using conventional modal analysis approach, it is possible to uncouple the governing equations using orthogonality properties of the mode shapes and thus evaluate the response based on the few dominate initial modes it requires the damping matrix to be proportional.

The state-space approach is another alternative which can not only simplify the formulation but is also suitable for the implementation of control strategies in semi-active systems to be explained later in next chapter. The state vector can be written as:

$$y = \begin{Bmatrix} \vec{x} \\ \dot{\vec{x}} \end{Bmatrix} \tag{0-3}$$

Now using Eq. (2-7), the governing equations of motion in Eq. (2-1) can be written using the following first-order differential equations:

$$\begin{bmatrix} \boldsymbol{C} & \boldsymbol{M} \\ \boldsymbol{M} & \boldsymbol{0} \end{bmatrix} \dot{\vec{y}} + \begin{bmatrix} \boldsymbol{K} & \boldsymbol{0} \\ \boldsymbol{0} & -\boldsymbol{M} \end{bmatrix} \vec{y} = \begin{Bmatrix} \vec{f} \\ 0 \end{Bmatrix} \tag{0-4}$$

where matrices $\boldsymbol{A}$ and $\boldsymbol{B}$ are defined as:

$$\boldsymbol{A} = \begin{bmatrix} \boldsymbol{C} & \boldsymbol{M} \\ \boldsymbol{M} & \boldsymbol{0} \end{bmatrix} \; and \; \boldsymbol{B} = \begin{bmatrix} \boldsymbol{K} & \boldsymbol{0} \\ \boldsymbol{0} & -\boldsymbol{M} \end{bmatrix} \tag{0-5}$$

The eigenvalue problem (free vibration) can then be written as

$$\boldsymbol{A}\dot{\vec{y}} + \boldsymbol{B}\vec{y} = \{0\} \tag{0-6}$$

Since the array $\vec{y}$ has *2n* elements, the solution to the above eigenvalue problem is a *2n* complex eigenvalues λ_r in a complex conjugate pairs and a *2n* complex eigenvectors $\{\theta\}_r$ (also complex conjugate pairs) [22]. For harmonic response, the eigenvalue problem in Eq. ((*0-6*) can be written as:

$$(\lambda_r \boldsymbol{A} + \boldsymbol{B})\{\theta\}_r = \{0\} \quad r = 1,2,\dots,2n \tag{0-7}$$

Since the state matrix $y = \begin{Bmatrix} \vec{x} \\ \dot{\vec{x}} \end{Bmatrix}$ represents the displacement and velocity vectors, the complex eigen vectors $\{\theta\}_r$ can be written as two vectors:

$$\{\theta\}_r = \begin{Bmatrix} \vec{\phi}_1 \\ \vec{\phi}_2 \end{Bmatrix}_r \tag{0-8}$$

where $\{\vec{\phi}_1\}_r$ reperesents the r^{th} displacement mode shape and $\{\vec{\phi}_2\}_r$ the r^{th} velocity mode shape. Substituting $\{\theta\}_r$ back into to the eigenvalue equation, Eq. ((*0-7*), results in:

$$\lambda_r \phi_1^r = \phi_2^r \xrightarrow{yields} \{\theta\}_r = \begin{Bmatrix} \phi \\ \lambda\phi \end{Bmatrix}_r \tag{0-9}$$

Eq. ((*0-9*) provides the relation between velocity and displacement mode shapes.

From the solution of the eigenvalue problem, Eq. ((*0-7*), the values of modal damping ratios and natural frequencies can be calculated as [23]:

$$\omega_{n,r} = |\lambda_r| \quad and \quad \zeta_r = \frac{-real(\lambda_r)}{|\lambda_r|} \tag{0-10}$$

It is noted that the matrix of complex eigenvectors $\boldsymbol{\theta}$ is orthogonal with respect to matrices $\boldsymbol{A}$ and $\boldsymbol{B}$ which can be mathematically described as:

$$\begin{aligned} \boldsymbol{\theta}^T \boldsymbol{A} \boldsymbol{\theta} &= [\nwarrow a_r \searrow] \\ \boldsymbol{\theta}^T \boldsymbol{B} \boldsymbol{\theta} &= [\nwarrow b_r \searrow] \end{aligned} \tag{0-11}$$

Since the rank of matrix $\boldsymbol{\theta}$ is *2n*, it can be used as a base of *2n*-dimensional space describing state vector y. The sate vector y can be transformed form physical to "generalized coordinates" defined by $\{q\}$ using the following relation:

$$\{y\} = \begin{Bmatrix} \vec{x} \\ \dot{\vec{x}} \end{Bmatrix} = [\boldsymbol{\theta}]\{q\} \tag{0-12}$$

Substituting Eq. (2-16), in the equation of the motion of the system in the state space form, Eq. ((*0-4*) and then pre-multiplying it from left side by $\boldsymbol{\theta}^T$, we can write the governing equation in the state space form with respect to generalized coordinates as:

$$\boldsymbol{\theta}^T \boldsymbol{A} \boldsymbol{\theta} \{\dot{q}\} + \boldsymbol{\theta}^T \boldsymbol{B} \boldsymbol{\theta} \{q\} = \boldsymbol{\theta}^T \begin{Bmatrix} \vec{f} \\ 0 \end{Bmatrix} \tag{0-13}$$

Since mode shape matrix $\boldsymbol{\theta}$ is orthogonal with respect to matrices $\boldsymbol{A}$ and $\boldsymbol{B}$, both terms on the left hand sides of Eq. (2-17) are uncoupled which provides a set of *2n* uncoupled first order equations as:

$$a_r\dot{q}_r + b_r q_r = F_r \qquad for\ r = 1,2,\dots,2n \tag{0-14}$$

where $F_r = \boldsymbol{\theta}^T \begin{Bmatrix} \vec{f} \\ 0 \end{Bmatrix}$

The derived uncoupled equations can now be transformed into the frequency domain using Fourier transform which yields:

$$\hat{Q}_r(j\omega) = \frac{\hat{F}_r(j\omega)}{(j\omega a_r + b_r)} \qquad for\ r = 1,2,\dots,2n \tag{0-15}$$

Reorganizing Eq. ((*0-15*) in a matrix form it can be expressed as

$$\{\hat{Q}(j\omega)\} = \boldsymbol{H_s}(j\omega)\{\hat{F}(j\omega)\} \tag{0-16}$$

where $\boldsymbol{H_s}$ is the frequency response function in the state space generalized coordinate as:

$$\boldsymbol{H_s}(j\omega) = diag\left[\frac{1}{(j\omega a_r + b_r)}\right]_{2n\times 2n}$$

By pre-multiplying Eq ((*0-16*) by[$\boldsymbol{\theta}$], one can bring back the transformed matrix from generalized coordinates to the physical coordinates as:

$$\boldsymbol{\theta}\{\hat{Q}(j\omega)\} = \boldsymbol{\theta H_s \theta}^T\{f(j\omega)\} \tag{0-17}$$

Defining $\boldsymbol{H_p}$ as

$$\boldsymbol{H_p}(j\omega) \equiv \boldsymbol{\theta H_s \theta}^T \tag{0-18}$$

Thus we can finally write:

$$\{\hat{Y}(j\omega)\} = \boldsymbol{H_p}(j\omega)\{\hat{f}\} \tag{0-19}$$

As it can be realized using this approach, we can evaluate the FRF matrix, $\boldsymbol{H_p}$ without evaluation of the inverse of an $n \times n$ matrix at each frequency. However, it should be noted that the matrix $\boldsymbol{H_p}$ here is a *2n×2n* matrix since the velocity mode shapes are also included in the matrix.

They can, however, simply be omitted when plotting the FRF graphs, since all the necessary information that is needed is already contained in the first $n \times n$ elements of the matrix [24]:

$$\{\hat{X}(j\omega)\} = \boldsymbol{H_p}(j\omega)_{n\times n}\{\hat{f}(j\omega)\} \tag{0-20}$$

Each element $H_{p_{ik}}$ in the matrix $\boldsymbol{H_p}$ represent the FRF of DoF i when a unit force is applied to the DoF *k*. Note that the matrix is also symmetric i.e. $H_{p_{ik}} = H_{p_{ki}}$. [25]

Error! Reference source not found. shows FRF for the fourth degree of freedom (subcomponent response) when the system is subject to unit impulse base excitation and the damping is un-proportional.

The values for masses and stiffness are taken from [8] and are considered to be:

$m_1 = 26112\ kg \qquad k_1 = 4\ \times 10^8\ \ N/m$

$m_2 = 18580\ kg \qquad k_2 = 1 \times 10^8\ \ N/m$

$m_3 = 1850\ \ kg \qquad k_3 = 1\ \times 10^{4.3}\ N/m$

$m_4 = 80 \qquad kg \qquad k_4 = 7.9\ \times 10^6\ N/m$

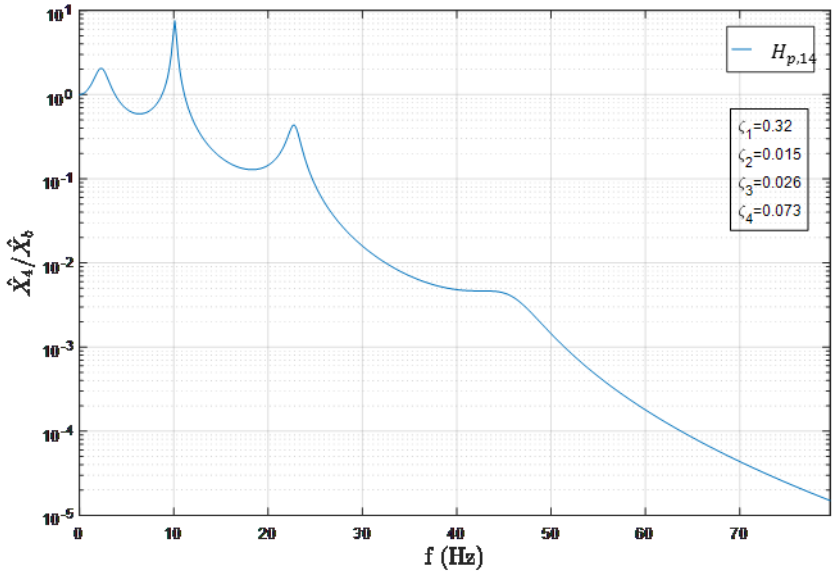

Figure 2.2: FRF of the 4th DoF for un-proportionally damped systems.

2.3 Frequency domain optimization

In the present work the main goal is to protect sensitive payload equipment from the base excitation. Therefore, the goal in the frequency domain can be defined as minimizing the absolute acceleration of the subcomponent ($\hat{\ddot{X}}_4$) (see Figure 2.1) within the frequency range of interest $[\omega_i - \omega_f]$. This is generally normalized with respect to the base acceleration ($\hat{\ddot{X}}_b$). The design needs to gurantee a certain working space, which is determined by the relative displacement between m_2 (reperesenting the 2nd stage of the LV) and m_3 (representing the payload).

Moreover, the frequency range of interest should be determined and the optimization in frequency domain needs to be conducted within the desired frequency range. As mentioned in the first chapter, generally for the design of the whole spacecraft vibration isolator, the main

concern is around the resonant burn frequency. The resonant burn for many launch vehicles for small payloads is around 50Hz [4], it is therefore a reasonable assumption to focus primarily on isolating the subcomponent for the frequencies within the range [40-60Hz].

In the modeling of the system, the dynamic characteristics of the isolator is generally reduced to two parameters, namely damping constant (c_3) and stiffness (k_3). With the above specifications, the optimization problem for passive isolation system in frequency domain can be formally formulated as follows:

Identify the optimal damping and stiffness parameters (c_3 and k_3) of the isolator separating the payload from the second stage of the launch vehicle to minimize the RMS value of the frequency response of the acceleration of the subcomponent ($\hat{\ddot{X}}_4$) normalized with respect to acceleration of the base ($\hat{\ddot{X}}_b$) within the frequency range $[\omega_i - \omega_f]$, The objective function as discussed in Chapter 1, can be mathematically defined as

$$f_{obj} = \sqrt{\frac{\int_{\omega_i}^{\omega_f} \hat{\ddot{X}}_4(\omega)^2 d\omega}{\int_{\omega_i}^{\omega_f} \hat{\ddot{X}}_b(\omega)^2 d\omega}} \tag{0-21}$$

The equality constraint is the equation of motion of the system transferred to frequency domain and written here in the matrix form as

$$h_1: \quad \boldsymbol{M}\left\{\hat{\ddot{X}}\right\} + \boldsymbol{C}\left\{\hat{\dot{X}}\right\} + \boldsymbol{K}\{\hat{X}\} = \boldsymbol{C}\left\{\hat{\dot{X}}_b\right\} + \boldsymbol{K}\{\hat{X}_b\} \tag{0-22}$$

where $\overrightarrow{\hat{X}_b} = \{\hat{X}_b, 0,0,0\}^T$, and $\boldsymbol{M}$, $\boldsymbol{C}$ and $\boldsymbol{K}$ matrices are described in Eq. (2-1).

The limits on the design are: 1-static deflection, which determines the lower limit of the isolator stiffness according to Eq. (1-1). Here the static deflection of $k_3$under the static load of the

payload and the subcomponent, assuming the system under goes 6g quasi-static acceleration in the vertical launch direction, can be described as

$$g_1: \qquad \delta_3 = \frac{(m_3 + m_4)6g}{k_3} \leq B \tag{0-23}$$

Where B is the allowable static deflection limit.

The RMS of the relative displacement between the LV and the payload in frequency domain can expressed as

$$g_2: \qquad \sqrt{\frac{1}{\omega_f - \omega_i}\int_{\omega_i}^{\omega_f}\left(\hat{X}_2 - \hat{X}_3\right)^2 d\omega} \leq A \tag{0-24}$$

where A is the upper limit for the RMS of the relative displacement, which is considered acceptable for design against fatigue failure of the components.

The design variables for designing the passive isolation system are c_3 and k_3. The rest of the stiffness and damping values are constant parameters determined by the structures of the LV and the payload. With this information the optimization problem can now be solved.

2.3.1 Optimization procedure

Having obtained the matrix $\boldsymbol{H_p}(j\omega)$ in the section 2.2 which relates the displacement vector to the excitation vector in frequency domain, it is now possible to solve the optimization problem formulated in previous section.

Here a method similar to the one recommended in [12] for optimization of an SDoF system is used and expanded to the present MDoF system. The acceleration of the 4th DoF can be written in terms of base acceleration, using the FRF matrix $\boldsymbol{H_p}(j\omega)$.

Recall from section 2.2, a forcing function, $\vec{\hat{f}}(\omega)$ can be defined as

$$\vec{\hat{f}}(\omega) = \boldsymbol{C}\left\{\dot{\hat{X}}_b\right\} + \boldsymbol{K}\{\hat{X}_b\} = \begin{Bmatrix} c_1\dot{\hat{X}}_b + k_1\hat{X}_b \\ \{\mathbf{0}\} \end{Bmatrix} \tag{0-25}$$

Therefore the displacement amplitude of the 4th DoF in the frequency domain is related to the base excitation as

$$\hat{X}_4(j\omega) = \left[H_{p_{41}}\, H_{p_{42}} \ldots\, H_{p_{44}}\right].\vec{\hat{f}}(\omega) = H_{p_{41}}\left(c_1\dot{X}_b + k_1 X_b\right) \tag{0-26}$$

And the frequency response function from the base displacement to the subcomponent displacement is obtained as

$$\frac{\hat{X}_4(j\omega)}{\hat{X}_b(j\omega)} = H_{p_{41}}(j\omega c_1 + k_1) \tag{0-27}$$

Using Eq. (0-27), the objective function in frequency domain as provided in Eq. ((*0-21*) can be expressed in terms of the FRF from the base to the subcomponenet displacement, $H_{p_{41}}$. Note that for linear system the displacement and acceleration ratios are identical (since for a linear system the acceleration signal can be expressed as $\ddot{X}_i(j\omega) = -\omega^2\hat{X}_i(j\omega)$). Therefore, the objective function in frequency domain can be expressed as

$$f_{obj} = \sqrt{\frac{\int_{\omega_i}^{\omega_f}\ddot{X}_4(\omega)^2 d\omega}{\int_{\omega_i}^{\omega_f}\ddot{X}_b(\omega)^2 d\omega}} = \sqrt{\frac{\int_{\omega_i}^{\omega_f}\left(\omega^2 H_{p_{41}}(j\omega c_1 + k_1)\hat{X}_b\right)^2 d\omega}{\int_{\omega_i}^{\omega_f}\left(\omega^2\hat{X}_b(j\omega)\right)^2 d\omega}} \tag{0-28}$$

From Eq. ((*0-28*), different cases of excitations can be readily analyzed. For the case of unit impulse acceleration of the base, ($\ddot{X}_b(\omega) = \omega^2 X_b(\omega) = 1$)) the objective function simplifies to

$$f_{obj} = \sqrt{\frac{1}{\omega_f - \omega_i}\int_{\omega_i}^{\omega_f}\left(H_{p_{41}}(j\omega c_1 + k_1)\right)^2 d\omega} \tag{0-29}$$

Similarly, for the unit impulse displacement of the base, $(X_b(\omega) = 1)$ the objective function in frequency domain becomes

$$f_{obj} = \sqrt{\frac{5}{\omega_f^5 - \omega_i^5} \int_{\omega_i}^{\omega_f} \left(\omega^2 H_{p_{41}}(j\omega c_1 + k_1)\right)^2 d\omega} \tag{0-30}$$

With the same procedure used for the derivation of the objective function based on the FRF matrix, it is possible to calculate the RMS value for the relative displacement between the payload and the LV within the same frequency range, represented as

$$\hat{X}_{23} = \left|\hat{X}_2 - \hat{X}_3\right| = \left|H_{p_{21}} - H_{p_{31}}\right| \hat{X}_b(j\omega c_1 + k_1) \tag{0-31}$$

So, the constraint function on relative displacement limit in frequency domain, described in Eq. (0-24), can be re-written as a function of base displacement $\hat{X}_b$ and the FRF matrix components as

$$g_2: \quad \sqrt{\frac{1}{\omega_f - \omega_i} \int_{\omega_i}^{\omega_f} \left(\hat{X}_b \left(H_{p_{21}} - H_{p_{31}}\right)(j\omega c_1 + k_1)\right)^2 d\omega} \leq A \tag{0-32}$$

Again the constraint g_2 can be calculated for the case of unit impulse acceleration and displacement of the base.

As it can be realized transfer function component $H_{p_{41}}$ has been used for the objective function while $H_{p_{31}}$ and $H_{p_{21}}$ are utilized for the evaluation of the constraint function. It is noted that elements of the matrix $\boldsymbol{H_p}$ are characteristics of the system and are independent of the excitation. Therefore, the frequency domain optimization of the isolator parameters is independent of the excitation to the system.

With the objective and constraint functions determined as a function of design variables, the optimization can be now carried out. As there are two design variables, here we can simply plot the contour of the objective function in the feasible design space specified by the constraint functions. Figure 2.3 shows the objective function contours and also the constraint functions. It is noted that for the contours are drawn with respect to the logarithm of design parameters, $\log(k_3)$ and $\log(c_3)$.

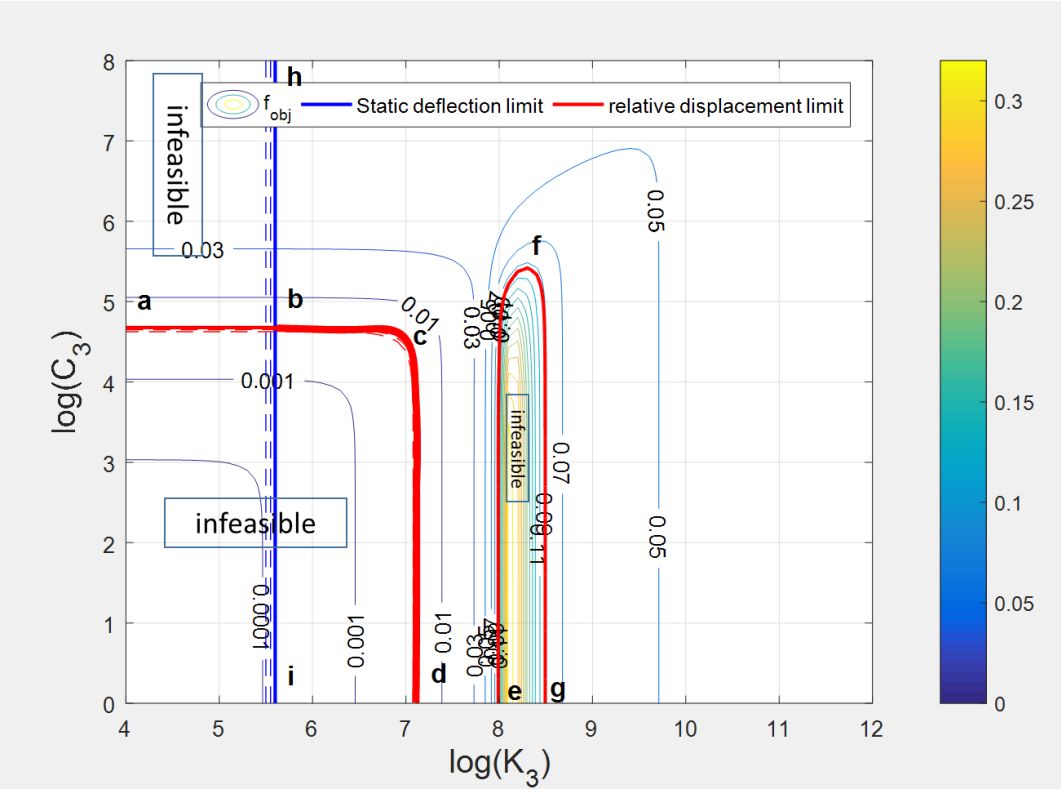

Figure 2.3: Contour of the objective function and the constraint equations in frequency domain

Examination of **Error! Reference source not found.** reveals that the objective function has the highest value around $\log(k_3) = 8.2$. The value of the relative displacement is also maximum around that point. The reason is that for $10^{8.1} < k_3 < 10^{8.4}$ the system will have two natural

frequencies within the frequency band where the objective function should be minimized [40-60 Hz]. To further clarify this, the four natural frequencies of the system are plotted vs variation of the isolator's stiffness in **Error! Reference source not found.**. As it can be seen, near $\log(k_3) = 8.2$, the third and fourth natural frequencies occur within the desired frequency band.

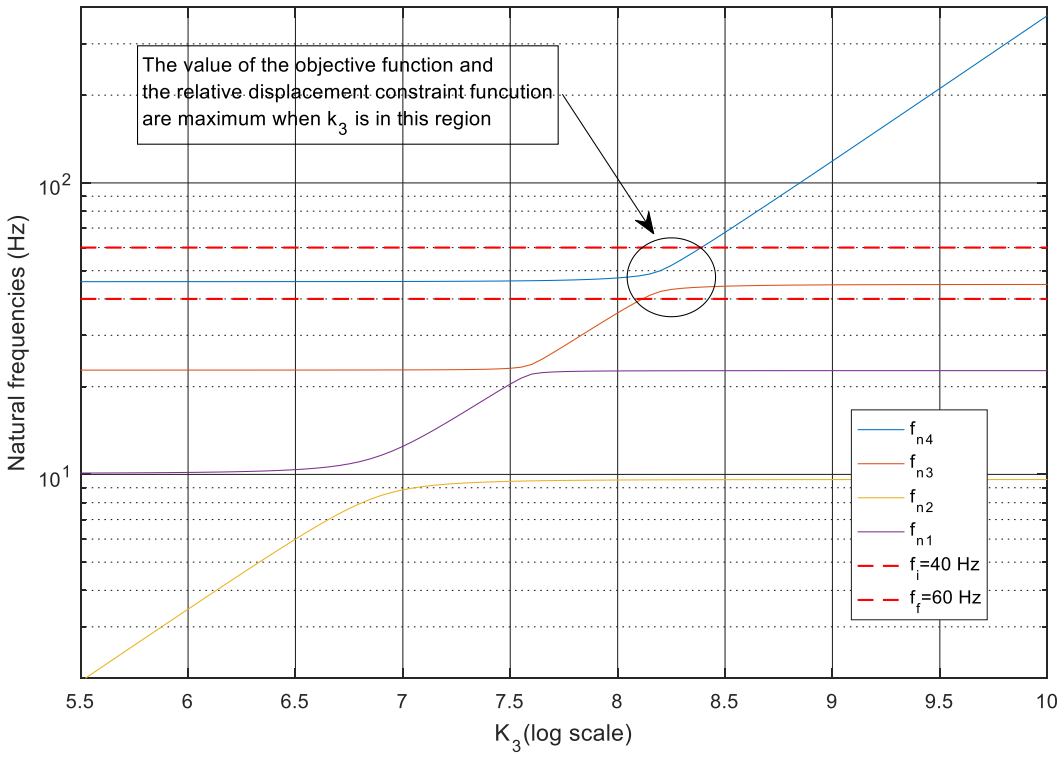

Figure 2.4: Variation of system natural frequencies with isolators' stiffness

It is noted that the optimal values for the objective function occurs when the contour of objective function coincides with relative displacement constraint function (a-b-c-d curve in Figure 2.3) further reducing the objective function will result in landing into the infeasible region. Thus all points on curve b-c-d represents the optimum solution as they minimize the objective function while satisfying all constraints. This again is due to the fact that the relative displacement and absolute acceleration are inversely proportional to each other in frequency domain.

Although same performance can be achieved with different values of isolator stiffness, from a practical point of view, the highest value on the optimum curve should be selected for the isolator stiffness as well as damping. The reason is that high stiffness and damping introduces less dynamics at low frequencies and offer a stronger connection between the two bodies. Here the value of $k_3^* = 10^{7.2}$ and $c_3^* = 10^{4.7}$is selected (point c in Figure 2.3)

Note that, even though a unique solution to the optimization problem of the passive system in the frequency domain does not exist, there exists a unique minimum for the objective function. This value can be used as the performance index to compare the performance of the semi-active isolator in frequency domain.

2.4 Time domain optimization

Although useful information regarding the dynamic characteristics of the system can be obtained through frequency analysis, it does not provide the maximum response. As it was discussed before the maximum response of the system which is of crucial importance for the isolator design, occurs before the transient part of the response damps out.

In Chapter 1, it was shown that for a single degree of freedom system, in frequency domain, the relative displacement between the base and the isolated mass is a monotonically decreasing function of stiffness and damping while the absolute acceleration of the isolated mass monotonically increases with the increase of stiffness and damping. However, the behavior of the system will be different when the analysis is done in time domain. To demonstrate this, consider the single degree of freedom system disused in section 1 as shown in Figure 2.5.

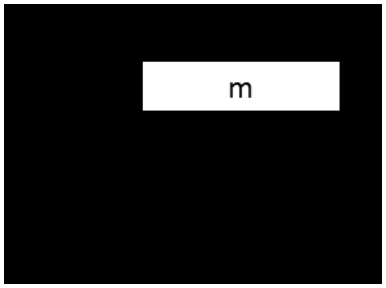

Figure 2.5:Passivley isolated SDoF system subject to base excitation

The governing equation of motion can be written as

$$\ddot{x} + 2\zeta\omega_n(\dot{x} - \dot{y}) + \omega_n^2(x - y) = 0 \tag{0-33}$$

Let us consider a case where the base excitation is described by velocity shock as

$$\dot{y} = \begin{cases} V_1 & t \leq t_0 \\ V_2 & t > t_0 \end{cases} \tag{0-34}$$

It is noted that a sudden change in the velocity of the base as described above, is equivalent to an impulse acceleration at t_0, thus "acceleration impulse" and "velocity shock" can be used interchangeably.

Error! Reference source not found. shows the normalized maximum absolute acceleration of the isolated mass as well as its maximum relative displacement, for different damping ratio, ζ under velocity shock described in Eq. (2-38).

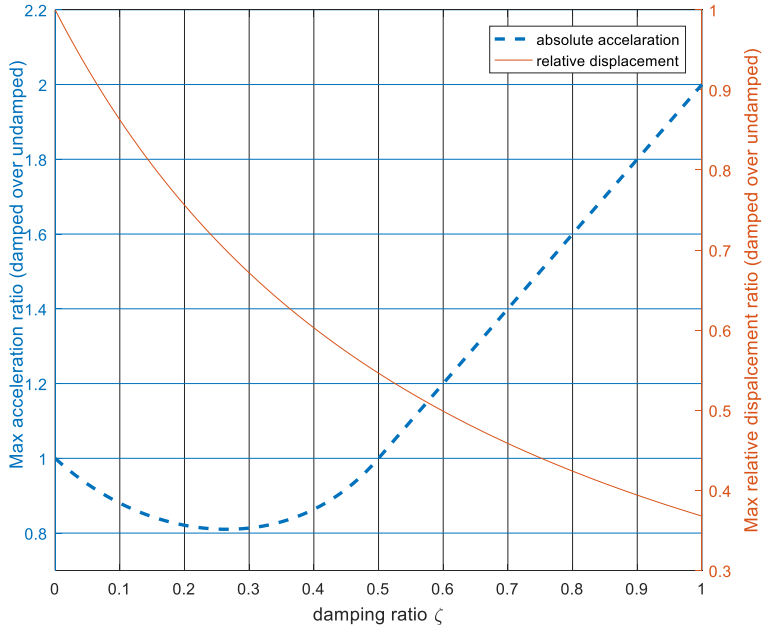

Figure 2.6: Acceleration and relative displacement response maxima for isolation system subject to velocity shock

As it can be seen, the absolute acceleration ratio (ratio of damped over undamped absolute acceleration of the isolated mass) decreases as damping ratio increases until it reaches to its minimum value of nearly 0.8 at the damping ratio of about 0.27 and then monotonically increases as damping ratio increases. It is noted that the absolute acceleration for the damped system is lower than that for the undamped system for the damping ratio less than 50%. Increasing damping ratio beyond 50% will cause the damped absolute acceleration to be actually greater than that of the undamped one. Maximum relative displacement however monotonically decreases as the damping ratio is increased.

Recall that in frequency domain, both relative displacement and absolute acceleration were varying *monotonically* and therefore there was no optimum for either function. The different

behavior of the system in time and frequency domain therefore necessitates the optimization to be carried out in both domains.

2.4.1 Formulation of the optimization problem in time domain:

Similar to section 2.3 the objective function can be defined as "minimizing the absolute acceleration of the payload, normalized with respect to acceleration of the base". In time domain the maximum response should be considered instead of the steady state part only. Therefore, the objective function in time domain can be defined as

$$f_{obj} = \frac{MAX\{|\ddot{x}_4(t)|\}}{MAX\{|\ddot{x}_b(t)|\}} \tag{0-35}$$

Similarly the equality constraint can be defined as the equation of motion of the system (in time domain)

$$h: \quad \boldsymbol{M}\ddot{\vec{x}} + \boldsymbol{C}\dot{\vec{x}} + \boldsymbol{K}\vec{x} = \boldsymbol{C}\dot{\overrightarrow{x_b}} + \boldsymbol{K}\overrightarrow{x_b} \tag{0-36}$$

The relative displacement between the LV and the payload in time domain can expressed as behavior constraint

$$g_2: \quad MAX\{|x_3(t) - x_2(t)|\} \leq A \tag{0-37}$$

It is noted that the inequality constraint g_1 in Eq. (2-27) for the frequency optimization remains the same for time domain optimization as well since it is a static limit.

2.4.2 Optimization procedure in time domain

In this section the result of time domain optimization when the system is subjected to unit impulse base acceleration excitation is investigated.

Error! Reference source not found. shows the peak value of absolute acceleration plotted vs maximum relative displacement for different value of stiffness and damping ratios.

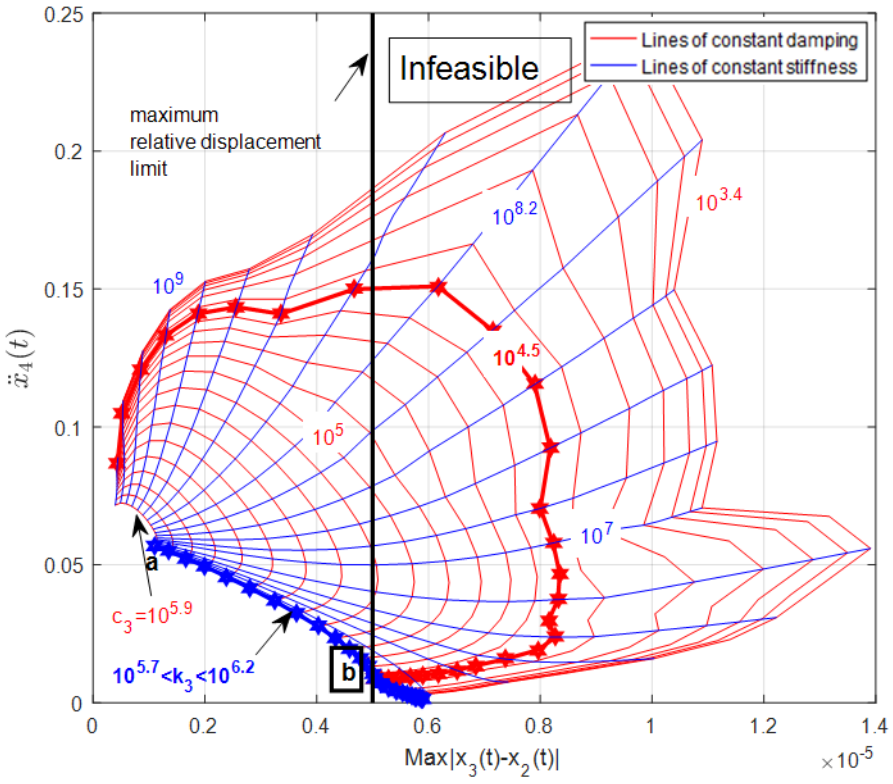

Figure 2.7: Peak value of absolute acceleration versus peak value of relative displacement when the system is subjected to unit impulse base acceleration

It is noted that for $10^{5.7} \leq k_3 \leq 10^{6.2}$ the lines of constant stiffness are coincident (shown by the curve $a-b$ in Figure 2.7). It indicates that for this range, the variation of k_3 has negligible effect on dynamics of the system. It can be seen from Figure 2.7, optimum solutions lie on the same curve $a-b$. It is noted that at point b on the curve, the value of absolute acceleration of the subcomponent is minimum while the relative displacement constraint is also satisfied and thus it is the optimum point. Point b however corresponds to range of $10^{5.7} \leq k_3 \leq 10^{6.2}$. The value of

the objective function on this design point can be used as the limit of time domain passive vibration isolation system to be compared with the semi-active ones.

Figure 2.8 also demonstrates contours of the objective function in the design space.

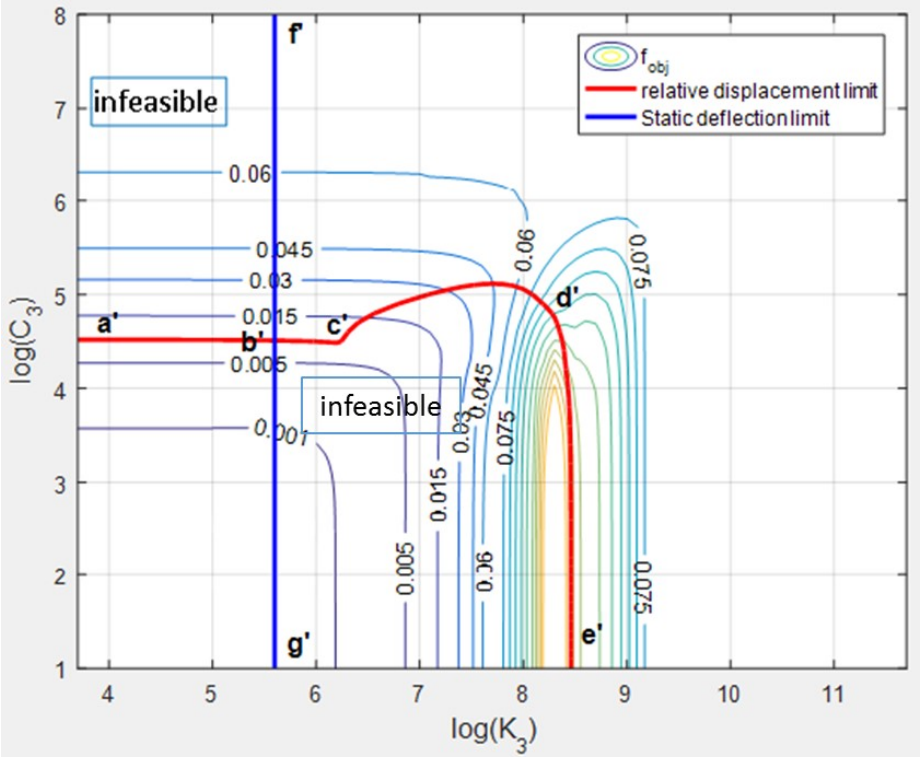

Figure 2.8: Peak value of absolute acceleration versus peak value of relative displacement when the system is subjected to unit impulse base acceleration

Similar to frequency domain optimization, there is no unique solution to the design optimization problem but there is an optimum design line $b' - c'$ where the value of the objective function will be minimum and the constraints are satisfied. This line corresponds to the same range of $10^{5.7} \leq k_3 \leq 10^{6.2}$ that was observed in Figure 2.7.

In Figure 2.8 point c' representing higher damping and stiffness have been selected as the optimum design point, thus $k_3^* = 10^{6.2}$ and $c_3^* = 10^{4.5}$. This is also comparable with optimal

value identified in Figure 2.7. As it can be realized the optimization in time domain has resulted in different optimum values compared with those in the frequency domain which found to be of $k_3^* = 10^{7.2}$ and $c_3^* = 10^{4.7}$.

2.5 Summery

In this chapter the characteristics of passive isolation system for the whole spacecraft was analyzed. Starting from the governing equation of motion of the system, a frequency response function (FRF) was found relating the base excitation to the displacement of the subcomponent. An optimization problem has been formulated in both time and frequency domain to minimize the absolute acceleration of the payload under relative displacement constraint. The isolator parameters were optimized in the frequency domain using the FRF matrix. The optimization procedure was then repeated in the time domain where the peak value of relative displacement between the LV and payload was used as the design constraint and the absolute acceleration of the subcomponent was used as objective function. The optimization did not yield a unique solution neither in time nor in frequency domain and there was a series of solutions (represented by an optimum curve rather than an optimum point) that would minimize the objective function and satisfy the constraint function in time and frequency domain. These values will be compared with results achieved in the next chapter, where the semi-active system based on variable damping constant is investigated.

CHAPTER 3: Semi-Active Isolator and its Effects on the Dynamics of the System

3.1 Introduction:

It was elaborated in detail in Chapter 1, that the passive isolation system cannot efficiently attenuate the acceleration response of the payload at the resonant peak without reduction in vibration isolation efficiency at higher frequencies. It was mentioned that this behavior of the passive isolation system is due to non-adaptability of the damping constant c for passive system. However, varying the damping constant, using adaptive devices can alleviate this shortcoming. Adaptive devices can be categorized into two main groups of fully active and semi-active systems. While fully active systems have shown superior performance in wide range of frequencies compared with passive systems, they have practical limitation due to complex control hardware and large power requirements. On the other hand semi-active systems have received growing interest recently as they provide the adaptability of the active systems while having fail-safe feature and reliability of the passive systems with low power requirements. Active dampers can effectively suppress the peak response at resonant frequency without the tradeoff of reduction in isolation performance at higher frequencies.

Semi-active dampers have proven to be efficient in attenuating the vibration transmitted to the isolated mass when the disturbances are harmonic or narrow-band (e.g. washing machine [27]) or when all dampers in system can be controlled (e.g. train isolation system [28]). This is not the case for the vibration isolation of the spacecraft however. Recall from section 1.2.5, the challenge when the goal is vibration isolation between two flexible bodies: the only variable is

the mechanical characteristics of the isolator and therefore the controllability over the system is limited.

In this chapter semi-active vibration isolation between a pair of flexible bodies representing the Launch Vehicle and the satellite will be examined. The main purpose of this chapter is to explore the feasibility of implementation of semi-active isolation system for LV/SC vibration isolation.

In the first part of this chapter an optimal control strategy is described followed by underlying assumptions. Then, the optimal control strategy has been implemented for the LV/SC model and results are obtained. These results are finally compared with those obtained for passive systems in Chapter 2, first in frequency domain and then in time domain.

3.2 Variable damping system

Although the idea of using variable damper to control the vibration goes back to almost a century ago, its practical implementation has a shorter history dating back to 1960s. In earlier types of variable dampers, hydraulic control was used to generate the controlled force, but since almost two decades ago, with the development of smart materials such as MR fluids, as well as accurate and inexpensive sensors and processors, the use of variable dampers became more widespread. This is mainly due to superior performance of MR base dampers and fast response (suitable for real-time control applications). Moreover these dampers do not have any movable parts (less wear).

Through this section the system is idealized to focus on the control algorithm with the assumption that regardless of the type of material that is used, the semi-active damper reacts immediately to the control signal (through changing its equivalent damping constant parameter) and therefore the system is not subject to any time delay. The second assumption is that the

damper is always capable of producing the required force. Thus, the results in this section can be understood as the best performance achievable with semi-active isolation system when compared to the passive case presented in the last chapter.

3.2.1 Skyhook control algorithm:

The Skyhook control algorithm is based on varying the damping constant, c in such way to replicate the effect of a damper that is located between the isolated mass and a fixed frame of reference (Sky). The problem is that a fixed frame of reference is generally not available and a semi-active damper is capable of exerting force only in the direction opposite to the relative motion between the base and the isolated mass and therefore the performance will never be as high as an ideal skyhook damper (which can only be achieved by an active system).

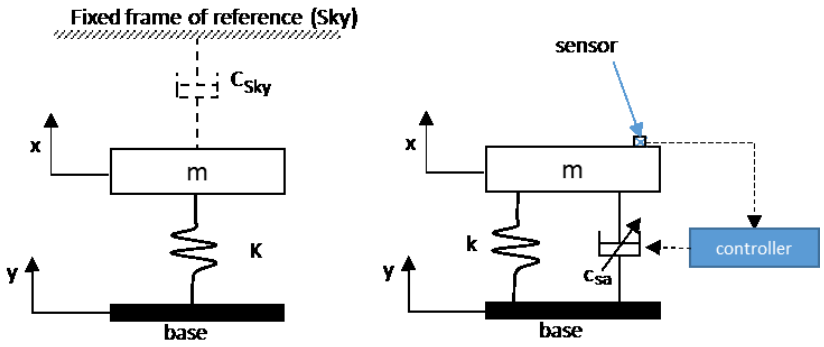

Figure 0.1: Skyhook damper ideal and semi-active

Karnopp [13] developed a strategy known as the Skyhook (SH) damping strategy to replicate the behavior similar to that of a skyhook damper. SH is the most commonly used strategy for semi-active damper isolation systems due to its simplicity and ease of practical implementation [31]. In its simplest form, it is based on a two state switching logic of the damping constant, c. The damping constant switches between two values, c_{MAX} and c_{min} (ideally equal to zero). The

switching logic is based on the absolute velocity of the isolated mass and the relative velocity between the isolated mass and the base. The SH damping strategy can be stated as [13]

$$c_{sa} = \begin{cases} c_{min} & \dot{x}(\dot{x} - \dot{y}) \leq 0 \\ c_{MAX} & \dot{x}(\dot{x} - \dot{y}) > 0 \end{cases} \tag{0-1}$$

The governing equation of motion of the SDoF system shown in Figure 0.1 can be described as

$$m\ddot{x} + c_{sa}(t)(\dot{x} - \dot{y}) + k(x - y) = 0 \tag{0-2}$$

It is noted that Eq. ((0-2) is nonlinear and therefore Fourier or Laplace transform cannot be used to transfer it to frequency domain. Here the concept of variance gain, introduced in section 1.2.6 should be used instead. As was shown in Chapter 1, the FRF and variance gain are identical for linear systems, like passive isolation system. Recall from section 1.2.6 that the approximate FRF for nonlinear systems can be calculated by subjecting the system to harmonic excitation $y_i = \sin(\omega_i t)$ then finding the *RMS* value of the response, $RMS(x_i)$ (the response can be acceleration, velocity, and displacement), and normalizing it by the RMS value of the excitation.

Figure 0.2 shows the approximate FRF for semi-active Skyhook system when the damping constant, ζ switches between the *on* state $(\zeta_{on} = 1)$ and the *off* state $\left(\zeta_{off} = 0.1\right)$ based on skyhook strategy stated in Eq. (3-1).

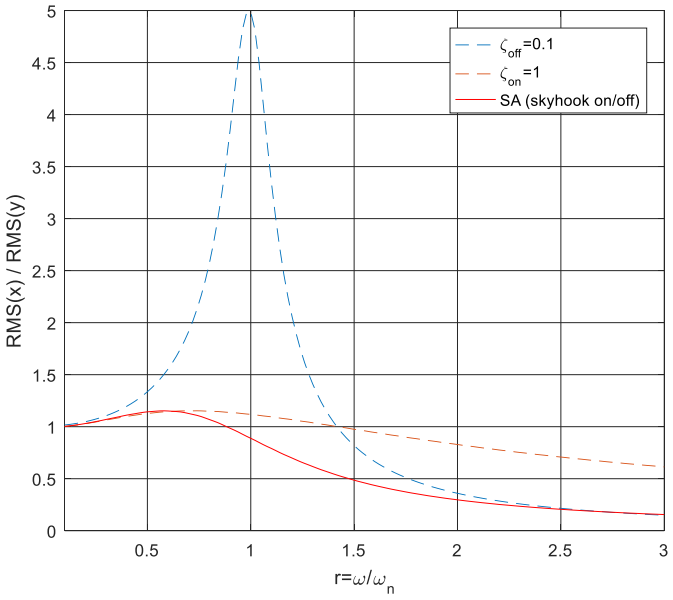

Figure 0.2: Approximate FRF of semi-active damper with SH control algorithm

It is clear from the Figure 3.2 that, the semi-active isolator with SH control is not subjected to the damping trade-off that the passive isolator typically experiences. That is to say it is able to reduce the peak at the resonance without any deterioration of the vibration isolation at higher frequencies.

3.2.2 ADD and SH-ADD control algorithm:

Savaresi [30] developed a control algorithm for a 2DoF system with semi-active dampers called Acceleration Driven Damper (ADD) control. Later, he combined the SH and ADD control algorithms to develop a semi-optimum control algorithm known as SH-ADD [31]. By semi-optimum it is meant that there is no better performance achievable with any damper working between c_{MAX} and c_{min}.

Savaresi [31] demonstrated that the acceleration response of the system at frequencies *above* the first resonance frequency of the system, can be attenuated more efficiently with ADD control when compared to SH control, while the SH control provides higher attenuation around the first resonant frequency. The idea of SH-ADD control is to combine the benefits of both control strategies. This control algorithm is briefly explained below using a 2DoF system used for car suspension system [30, 31] subjected to base excitation as shown in Figure 0.3.

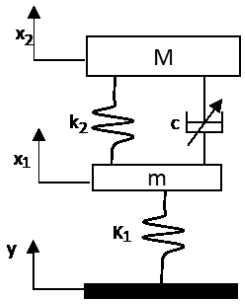

Figure 0.3: Schematic representation of 2DoF car suspension system

In ADD algorithm the switching logic is based on the absolute acceleration of the sprung mass (M) and the relative velocity between the sprung and the unsprung mass (m) as

$$c_{sa} = \begin{cases} c_{min} & \ddot{x}_2(\dot{x}_2 - \dot{x}_1) \leq 0 \\ c_{MAX} & \ddot{x}_2(\dot{x}_2 - \dot{x}_1) > 0 \end{cases} \tag{0-3}$$

In [31] it is shown that the semi-optimum damping can be achieved by combining the SH and ADD damping strategies.

Since SH control algorithm is more efficient at lower frequencies while ADD is better at higher frequencies, this method can be viewed as a switching mechanism between ADD algorithm and SH algorithm at different frequencies so that the most efficient strategy at each frequency range

is applied. It is first necessary to find the cross-over frequency denoted by α and then switch between the two strategies at the cross-over frequency. This can be expressed as [31]:

$$\begin{cases} use\ SH\ if & (\ddot{x}_2^2 - \alpha^2 \dot{x}_2^2) < 0 \\ use\ ADD\ if & (\ddot{x}_2^2 - \alpha^2 \dot{x}_2^2) > 0 \end{cases} \tag{0-4}$$

where α is the cross-over frequency.

In Figure 0.4 and Figure 0.5, the performance of SH-ADD control algorithm is shown and compared with SH and ADD algorithms individually as well as passive system. The higher performance of SH control strategy around the first resonant frequency and the benefits of ADD control strategy around the second frequency is evident. As it can be realized SH-ADD strategy combines the advantages of both control strategies and is capable of attenuating vibration in wide range of frequencies

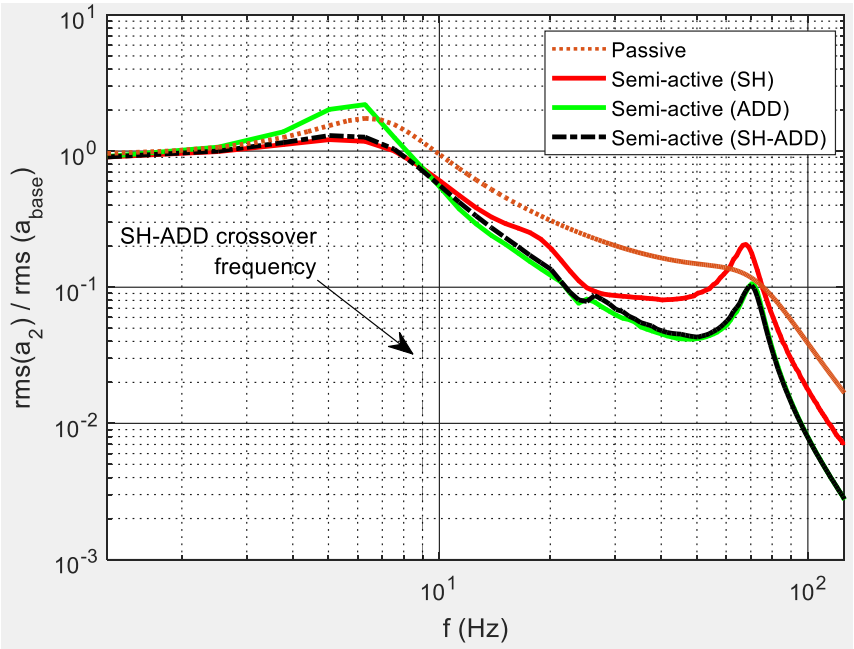

Figure 0.4: The acceleration response of SH, ADD and SH-ADD controls

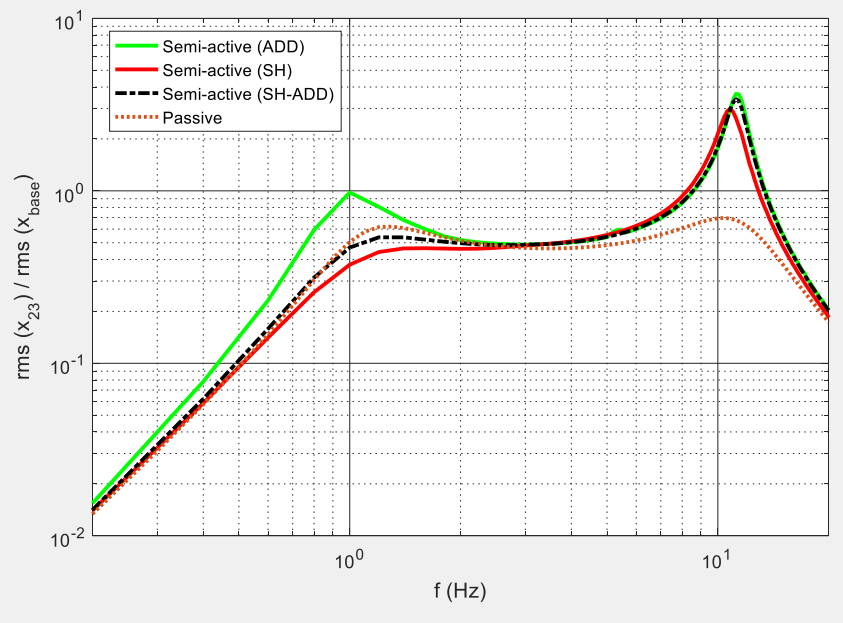

Figure 0.5: The relative displacement when SH, ADD and SH-ADD control is used

3.3 Implementation of semi-active damper design to LV/SC system:

Here the passive damper c_3 in the LV/SC system is replaced with a semi-active damper, $c_{3,sa}$, and a procedure similar to that described in chapter 2 is followed to derive the value of the performance index. Figure 0.6 shows the model of the system when the passive isolator is replaced with a semi-active one. The equation of motion of the system with semi-active damper is provided in Eq. ((0-5).

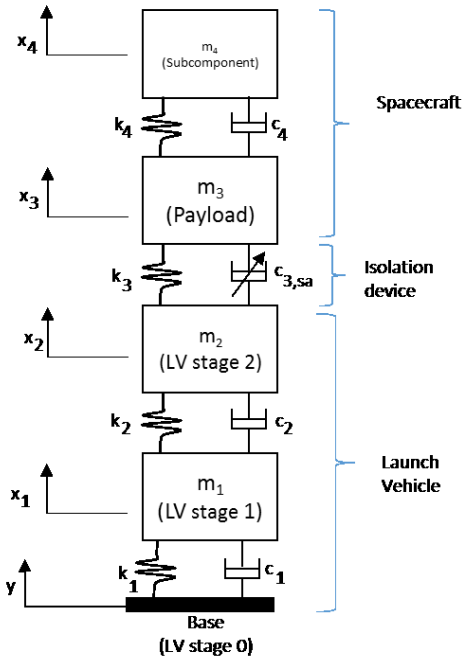

Figure 0.6: Schematic of LV/SC system when semi-active isolator is used

$$M\ddot{\vec{x}} + \begin{bmatrix} c_1 + c_2 & -c_2 & & \\ -c_2 & c_2 + c_{3,sa} & -c_{3,sa} & \\ & -c_{3,sa} & c_{3,sa} + c_4 & -c_4 \\ & & -c_4 & c_4 \end{bmatrix} \begin{Bmatrix} \dot{x}_1 \\ \dot{x}_2 \\ \dot{x}_3 \\ \dot{x}_4 \end{Bmatrix} + K\vec{x} = \begin{Bmatrix} c_1\dot{y} + k_1 y \\ 0 \\ 0 \\ 0 \end{Bmatrix} \tag{0-5}$$

$$\boldsymbol{M}\ddot{\vec{x}} + \boldsymbol{C}_{sa}\dot{\vec{x}} + \boldsymbol{K}\vec{x} = \vec{f}$$

Recall from chapter 2 that the value of the objective function in frequency domain was calculated by: first deriving the FRF of the subcomponent when the system is subjected to base excitation, $H_{p,14}$, then calculating the RMS of the acceleration signal of the subcomponent based on the frequency response function, $H_{p,14}$ within the frequency range of interest of [40-60] Hz.

Here, the same procedure will be fallowed for the semi-active system, the difference is that for the nonlinear semi-active system described by Eq. ((0-5) the frequency response function is not defined and therefore the approximate FRF (based on variance gain) has to be used.

3.3.1 Implementation of semi-optimal control

Here the concept of SH-ADD damping introduced in section 3.2.2 is used as the control strategy to vary the value of $c_{3,sa}$ damper. The procedure to use SH-ADD control is first to plot the approximate FRF of the isolated mass (here m_4) when the SH strategy is used, then repeat the procedure using ADD control strategy. Then the cross-over frequency, α can be determined to use in the final control law described in Eq. ((0-4).

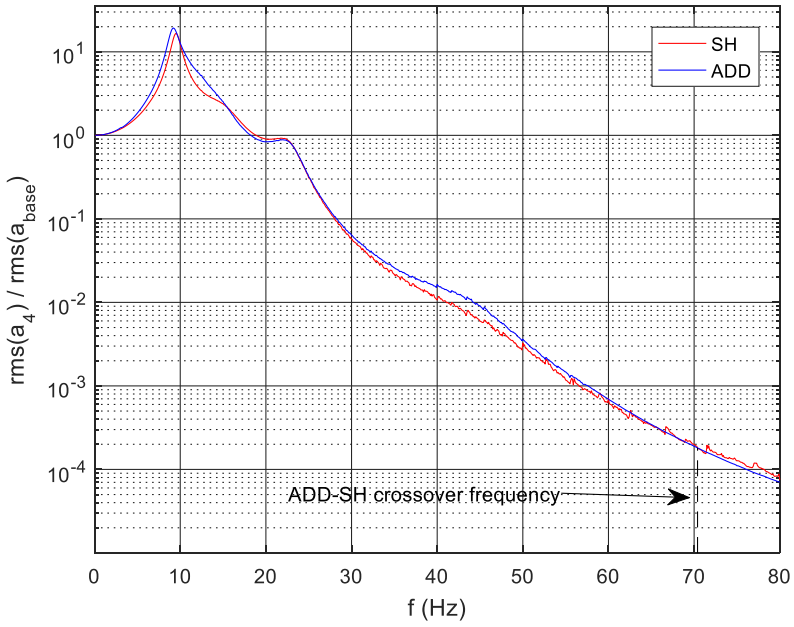

Figure 0.7: Approximate FRF of the 4th DoF for ADD and SH control.

Figure 0.7 show that the crossover occurs at a frequency about 70 Hz. Thus, the cross-over frequency is beyond the frequency range of interest of 40 to 60Hz, within which the SH strategy has a better performance in reducing the absolute acceleration of the subcomponent.

In Figure 0.8 the RMS value of the relative displacement between the 2nd and 3th DoF is plotted when SH and ADD control algorithms are used. It can be seen that SH has also a better effect on reducing the relative displacement compared to ADD within frequency range of interest

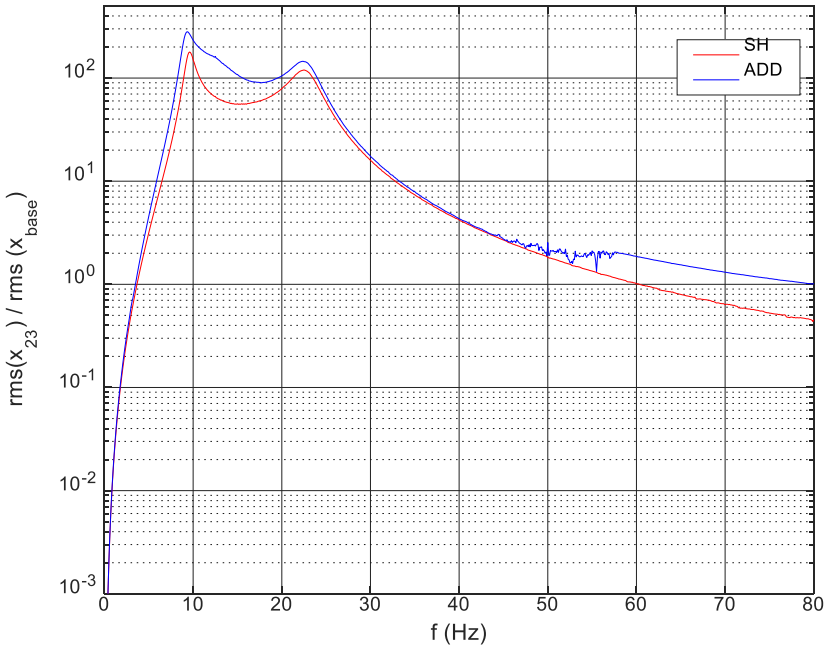

Figure 0.8: RMS of relative displacement, x_{23} when ADD and SH control is used

3.4 Comparison of optimum passive with semi-active isolator design in frequency domain

As shown in previous section SH semi-active control strategy has shown better performance compared to SH-ADD control strategy in the frequency range of interest. Here the performance of the SH semi-active control strategy has been compared with those of optimal passive systems in Chapter 2. Figure 0.9 shows the results for the RMS absolute acceleration of the 4th DoF using semi-active and optimum passive isolators.

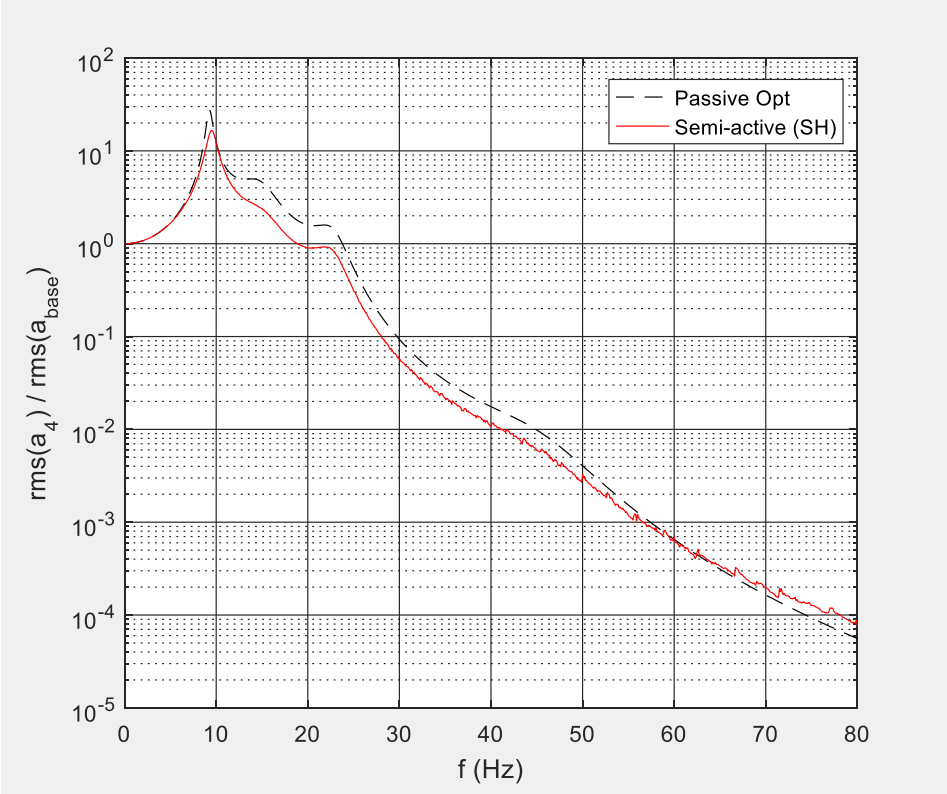

Figure 0.9: Acceleration response of the 4th DoF with passive and semi-active isolators

Figure 0.10 also shows the relative displacement between the LV and the payload in frequency domain using SH semi-active and optimum passive isolators.

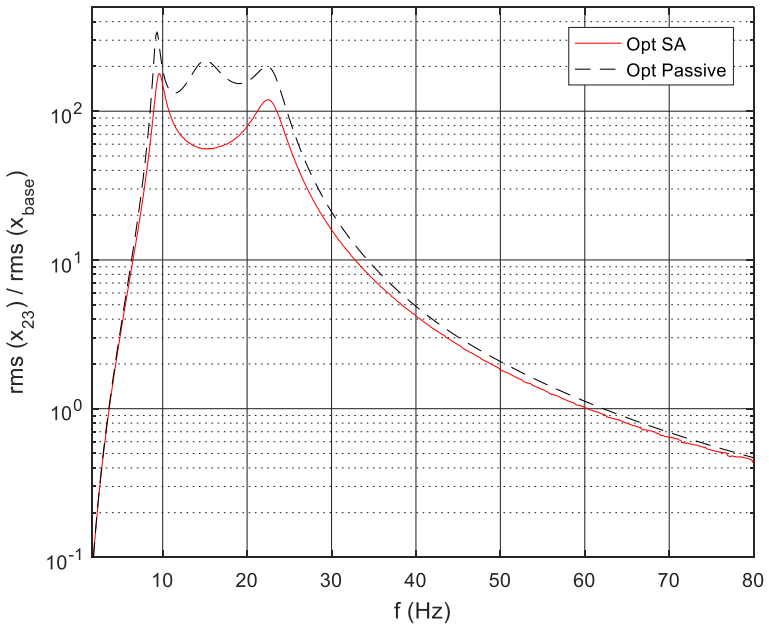

Figure 0.10: Relative displacement x_{23} rms, when passive and semi-active system are used

As it is clear from Figures 3.9 and 3.10, the semi-active system has a better performance compared with passive system in the whole frequency range. This can be quantified by returning to the objective function and constraint functions introduced in Eq. ((*0-21*) and Eq. ((*0-24*) respectively.

Recall that the objective function in Eq ((*0-21*) represents the RMS value of the steady state acceleration response of the 4th DoF, normalized with respect to RMS of the base acceleration. Figure 3.11 shows the RMS absolute acceleration of the 4th DoF normalized with respect to that for the base in the frequency range of 40-60 Hz for both SH semi-active and optimal passive systems.

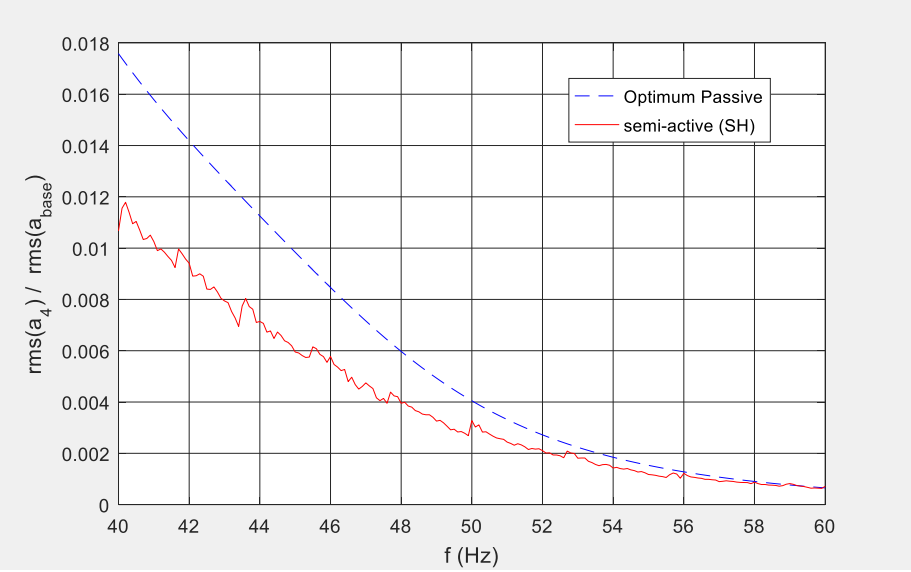

Figure 0.11: The area under each curve represents the value of the objective function

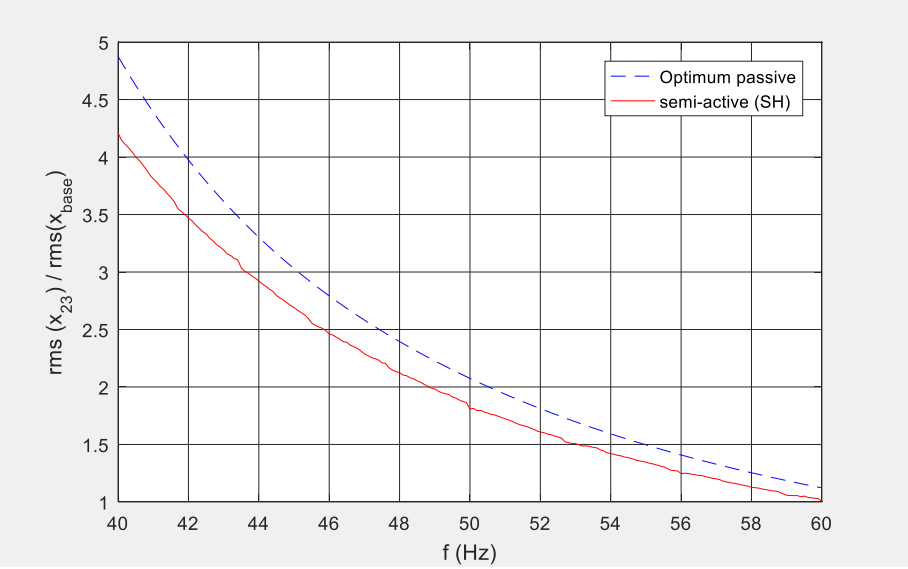

Figure 0.12: The area under each curve represents the value of relative displacement constraint function

It is noted that the area under the red curve in Figure 3.11 is the value of the objective function for semi-active system and the area under the blue curve is the value of the objective function for the optimized passive system. Using semi-active control, the performance is improved by 32%

within the frequency range of [40-60Hz] while the relative displacement is reduced by 11.7% within the same frequency range.

It can therefore be concluded that, using semi-active damper can significantly increase the performance of the isolator, while simultaneously reduces the relative displacement between the payload and the lunch vehicle in the desired frequency range. However, these results are valid when the excitation is assumed to be narrow band or harmonic signal. The performance of isolators under random broadband excitation is discussed latter in this chapter.

3.5 Time domain comparison of passive and semi-active isolation systems

To compare the performance of the semi-active with passive isolation system in the time domain, the optimized design of the passive isolator in the time domain, presented in section 2.4.2, is used as the base line for this section. Similar to the passive system, the semi-active system is subjected to a unit impulse base acceleration and the absolute acceleration of the subcomponent ($a_4(t)$) and relative displacement between the LV and the payload ($x_{23}(t)$) are obtained. Figure 0.13 Figure 0.14 show the results for the absolute acceleration and relative displacement for the passive and semi-active systems, respectively.

The results show that in time domain the semi-active system does not decrease the peak value of the absolute acceleration or relative displacement. The peak values remain essentially unchanged. It is noted that a higher frequency component appears in the acceleration response of the sub component when semi-active system is used. These higher frequency components are mainly due to the nonlinearities induced by using semi-active damper. As mentioned in section 3.2, the damping constant $c_{3,sa}$ is switching between two values based on the control strategy stated in Eq. (3-4) which introduces an additional component to the acceleration response signal

of the 4th DoF (a_4) [29]. Examination of results reveal that for cases in which the system is under impact the semi-active control strategy does not provide advantage in reducing the peak response compared with optimal passive system.

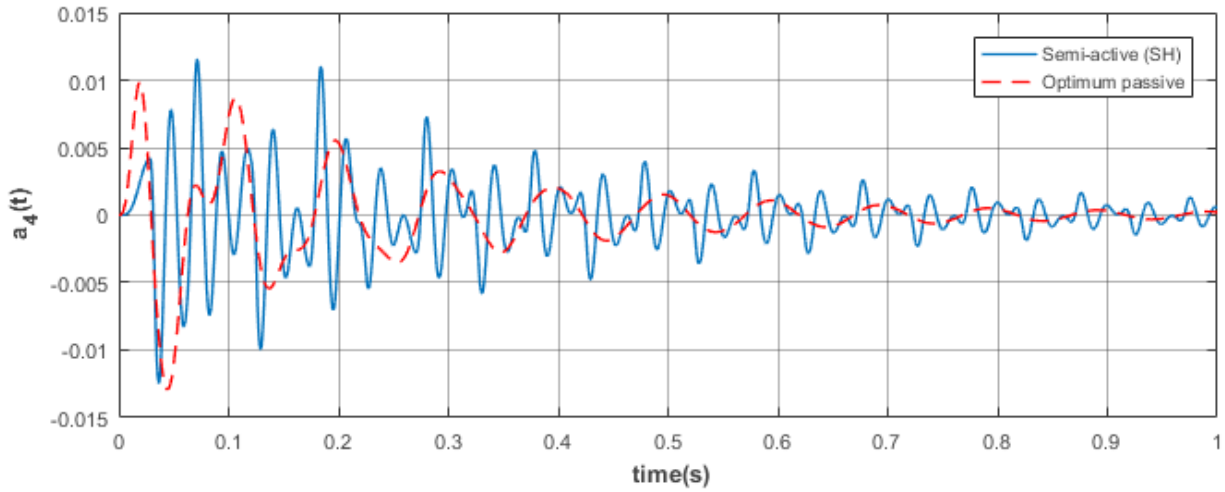

Figure 0.13: Absolute acceleration of the 4th DoF when semi-active and passive isolator is used

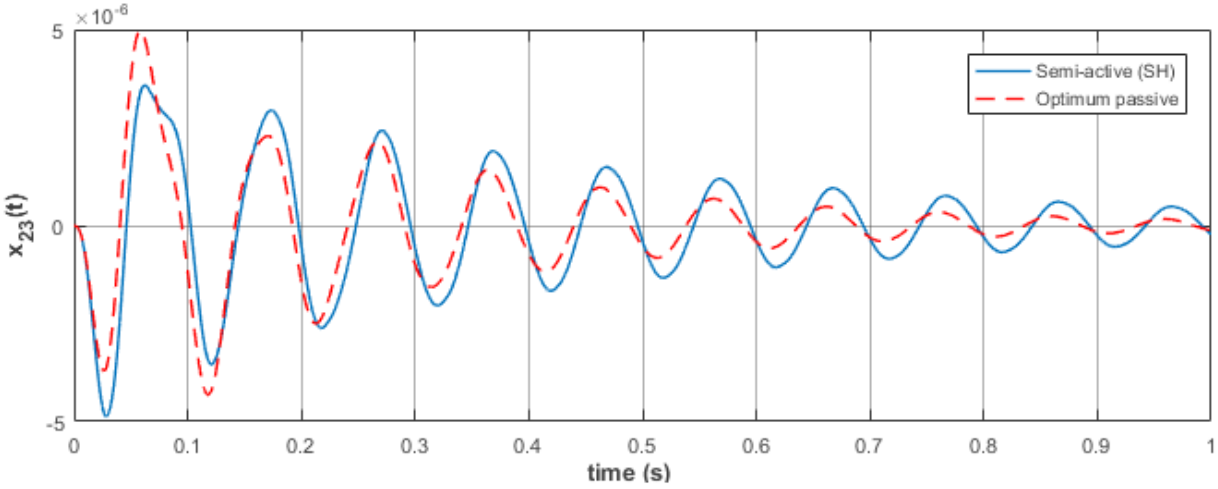

Figure 0.14: Relative displacement between the 2nd and the 3rd DoF when semi-active and passive isolator is used

3.6 Comparison of passive and semi-active isolators when the system is subjected to random broadband excitation

So far the analysis of the system was limited to the cases where the base excitation was harmonic or unit impulse. In this section both semi-active and passive system will be subjected to broadband random excitation to compare their performance when subjected to a realistic model of the launch environment. Broadband random excitation is modeled here by white noise[2].

As mention in Chapter 1, the Power Spectral Density (PSD) will be used to compare the performance of passive and semi-active system when the excitation is in the form of stationary random. Figure 0.15 shows the PSD of the acceleration of the 4^{th} DoF (subcomponent) for both cases of optimal passive and semi-active isolators.

[2] White noise is defined as a signal with equal energy at all frequencies, therefore its PSD representation will be a straight line.

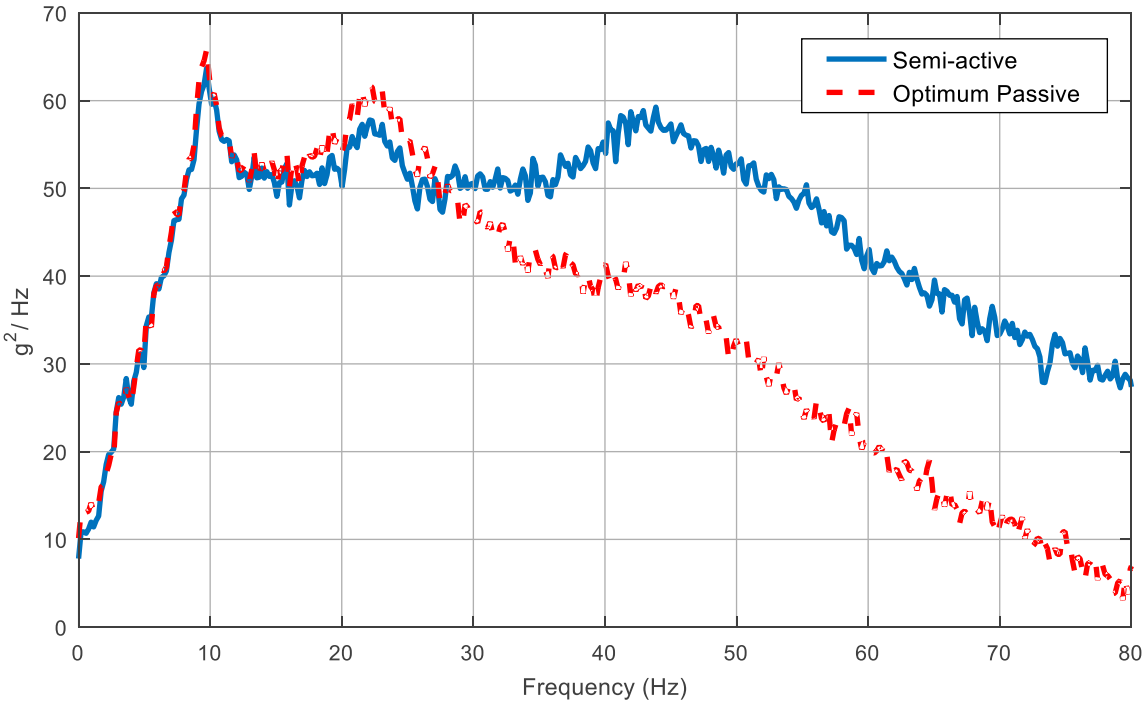

Figure 0.15: PSD of absolute acceleration of the subcomponent (a_4) for passive and semi-active system

It can be seen that although the semi-active damper improves the response around the resonant frequencies, but at higher frequencies its performance is deteriorated compared to passive isolator.

3.7 Some remarks regarding semi-active damping of MDoF system

Here it is worth taking a closer look at Figure 0.2, which shows the improvement that can be achieved when semi-active isolator is used to protect an SDoF payload, and compare it with Figure 0.9, which shows the performance of semi-active isolator when used in an MDoF system representing the LV/SC under harmonic excitation. These figures are reproduced below in Figure 3.16 for the sake of clarity.

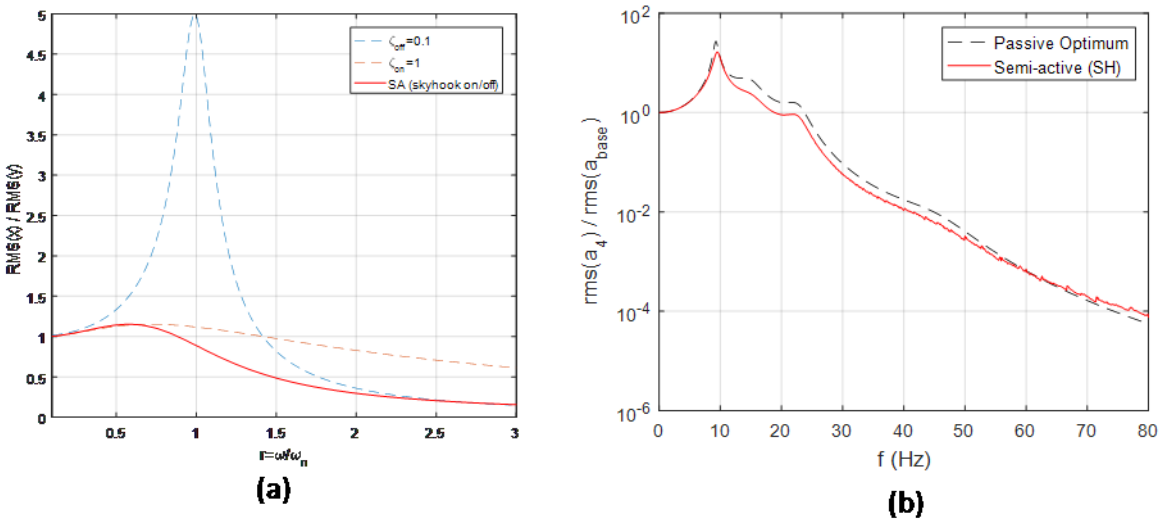

Figure 0.166: Comparison of passive and semi-active isolator when the system is: (a) SDoF and (b) MDoF representing LV/SC

Figures 3.16 (a) and (b) show that semi-active system is more effective to isolate vibration for an SDoF system compared with that of MDoF system. This can be attributed to the fact that in SDoF modal damping ratio is directly proportional to the damping coefficient ($\zeta = \frac{c}{2\sqrt{mk}}$), thus control strategy has the full authority to vary the damping ratio over broad range, however in the MDoF system varying the damping coefficient between the payload and the launch vehicle would affect all modal damping ratios and not just the damping ratio associated with that damping coefficient. This subsequently reduces the authority of the semi-active control strategy for the MDoF systems.

3.8 Summery

In this chapter semi-active damping strategy for vibration isolation of the subcomponent in payload/ launch system was analyzed, first in frequency and then in time domain and the results were then compared with optimum passive design developed in the previous chapter.

The analysis showed that the benefit of using the semi-active system in frequency domain is significant. It however, showed that in time domain the effects are not as promising since the peak value of relative displacement and absolute acceleration is used as performance index, and both these values remain fundamentally unchanged when semi-active system is used. Later the semi-active and passive isolator performances were compared when the excitation is random and broadband. PSD of the absolute acceleration of the isolated mass was used to compare the performance and the results showed that the benefit that semi-active system brings around resonant frequencies are compromised by the reduction in isolator's performance at higher frequencies. Finally, the fundamental reason behind the fact that the semi-active system produces less promising results when the system is a more complicated MDoF compared to a simpler SDoF system are discussed and it was shown that this behavior is due to the fact that in a MDoF system, even with the assumption of full control over damping constants, it is impossible to control the damping ratios fully and independently.

CHAPTER 4: Conclusion

4.1 Major contributions:

The main focus of the present research study was to fundamentally study the vibration response of a coupled launch vehicle (LV) and spacecraft (SC) system modeled as a pair of flexible structures each with multiple natural frequencies and vibration modes, connected to each other via an isolator. Both passive and semi-active systems have been investigated and their performance in frequency and time domain has been compared. Moreover, an investigation was conducted to identify the optimal passive isolation systems with respect to its stiffness and damping properties. The major contributions of this research study can be summarized as:

- Development of a methodology for design optimization of passive vibration isolation system between pair of flexible bodies in both frequency and time domain.
- Modifying an optimal control strategy for the MDoF system representing the LV/SC.

4.2 Major conclusions

The main conclusions of the present work are enumerated bellow:

- Semi-active isolation systems can significantly reduce the vibration transmitted to the payload when harmonic or narrow band base excitation is considered.
- When considering the peak value of the absolute acceleration of the payload and the peak value of the relative displacement between the isolated body and the base (time domain analysis), the results showed that the semi-active system does not improve the performance of the system when compared to an optimally designed passive isolation system.

- The response to random excitation showed that while the semi-active damper can improve the performance of the isolator around resonant peaks, passive isolator is better at attenuating the vibrations at higher frequencies. This was due to nonlinearities that the semi-active isolator introduces to the system.
- The results suggests that, unlike systems with high degree of controllability over its dynamic characteristics, the use of semi-active damper is not as promising when the system is more complicated with multiple degrees of freedom and the mechanical environment is random and broadband, even when the semi-active system is idealized by neglecting the time delay and force limitation inherent in semi-active systems.

4.3 Recommendation for future work

Limited studies have been conducted on vibration and shock isolation of the space payload (spacecraft) and subcomponents under launch environment. This study attempted to do some fundamental study on this topic in order to better understand the effect of isolation system between the payload and launch vehicle on the response of the subcomponents. Some of the areas that can be further investigated in future work are:

- An experimental test to compare the results of passive and semi-active vibration isolation of the payload when the system is flexible on both sides of the isolator.
- Further investigation into vibration isolation of MDoF systems with un-proportional damping to develop more accurate models to mathematically model the un-proportionally damped systems.
- Investigate other options such as semi-active with variable damping and stiffness or fully active systems to attenuate the vibration transmission to the payload.

References

1. Wilke, P., et al. *Whole-spacecraft vibration isolation for broadband attenuation*. in *Aerospace Conference Proceedings, 2000 IEEE*. 2000. IEEE.
2. Wijker, J.J., *Random vibrations in spacecraft structures design: theory and applications*. Vol. 165. 2009: Springer Science & Business Media.
3. Secretariat, E., *Spacecraft mechanical loads analysis handbook.* 2013.
4. Johnson, C.D., P.S. Wilke, and P.J. Grosserode. *Whole-spacecraft vibration isolation system for the GFO/Taurus mission*. in *1999 Symposium on Smart Structures and Materials*. 1999. SPIE.
5. Liu, L., G. Zheng, and W. Huang, *Octo-strut vibration isolation platform and its application to whole spacecraft vibration isolation.* Journal of sound and vibration, 2006. **289**(4): p. 726-744.
6. Likun, L., Z. Gangtie, and H. Wenhu, *Study of liquid viscosity dampers in octo-strut platform for whole-spacecraft vibration isolation.* Acta Astronautica, 2006. **58**(10): p. 515-522.
7. Zheng, G., *Parametric studies of the whole spacecraft vibration isolation.* AIAA journal, 2003. **41**(9): p. 1839-1841.
8. Liu, L., et al., *Dynamic design of octostrut platform for launch stage whole-spacecraft vibration isolation.* Journal of spacecraft and rockets, 2005. **42**(4): p. 654-662.
9. Liu, L. and G. Zheng, *Parameter analysis of PAF for whole-spacecraft vibration isolation.* Aerospace science and technology, 2007. **11**(6): p. 464-472.
10. Johal, R., P. Wilke, and C. Johnson, *Rapid Coupled Loads Analysis and Spacecraft Load Reduction using SoftRide.* 2009.
11. Evert, M.E., et al., *Active vibration isolation system for launch load alleviation*. 2004, CSA ENGINEERING INC MOUNTAIN VIEW CA.
12. Jazar, G.N., et al., *Practical frequency and time optimal design of passive linear vibration isolation mounts.* Vehicle system dynamics, 2003. **39**(6): p. 437-466.
13. Karnopp, D., M.J. Crosby, and R. Harwood, *Vibration control using semi-active force generators.* Journal of engineering for industry, 1974. **96**(2): p. 619-626.
14. Muhammad, A., X.-l. Yao, and Z.-c. Deng, *Review of magnetorheological (MR) fluids and its applications in vibration control.* Journal of Marine Science and Application, 2006. **5**(3): p. 17-29.
15. Jean, P., R. Ohayon, and D. Bihan. *Semi-active control using magneto-rheological dampers for payload launch vibration isolation*. in *SPIE symposium on smart structures and materials*. 2006.
16. Jean, P., *Isolation vibratoire par contrôle semi-actif d'amortisseurs magnéto-rhéologiques pour l'interface lanceur/charge utile*. 2006, Conservatoire national des arts et metiers-CNAM.
17. Jean, P., P. Gardonio, and B. Mace, *Semi-active isolation of a single degree-of-freedom system using a magneto-rehological damper.* 2005.
18. Zheng, G. and Y. Tu, *Analytical study of vibration isolation between a pair of flexible structures.* Journal of vibration and acoustics, 2009. **131**(2): p. 021006.
19. Karahalis, G.G., *Whole Spacecraft Vibration Isolation*. 1999, AIR FORCE INST OF TECH WRIGHT-PATTERSONAFB OH SCHOOL OF ENGINEERING.
20. Jarosh, J.R., *Active and adaptive control for payload launch vibration isolation*. 2000, AIR FORCE INST OF TECH WRIGHT-PATTERSONAFB OH SCHOOL OF ENGINEERING.
21. Preumont, A., *Vibration control of active structures: an introduction*. Vol. 179. 2011: Springer Science & Business Media.
22. Ewins, D.J., *Modal testing: theory and practice*. Vol. 15. 1984: Research studies press Letchworth.
23. Lallement, G. and D.J. Inman. *A tutorial on complex eigenvalues*. in *PROCEEDINGS-SPIE THE INTERNATIONAL SOCIETY FOR OPTICAL ENGINEERING*. 1995. SPIE INTERNATIONAL SOCIETY FOR OPTICAL.

24. Beliveau, J.-G. and Y. Soucy, *Damping synthesis using complex substructure modes and a Hermitian system representation.* AIAA journal, 1985. **23**(12): p. 1952-1956.
25. Fu, Z.-F. and J. He, *Modal analysis*. 2001: Butterworth-Heinemann.
26. Wilke, P., C. Johnson, and P. Grosserode, *GFO/Taurus whole-spacecraft vibration isolation system.* 1998.
27. Chrzan, M.J. and J.D. Carlson. *MR fluid sponge devices and their use in vibration control of washing machines*. in *SPIE's 8th Annual International Symposium on Smart Structures and Materials*. 2001. SPIE.
28. Liao, W. and D. Wang, *Semiactive vibration control of train suspension systems via magnetorheological dampers.* Journal of intelligent material systems and structures, 2003. **14**(3): p. 161-172.
29. Ahmadian, M., B. Reichert, and X. Song, *System non-linearities induced by skyhook dampers.* Shock and Vibration, 2001. **8**(2): p. 95-104.
30. Savaresi, S.M., E. Silani, and S. Bittanti, *Acceleration-Driven-Damper (ADD): An optimal control algorithm for comfort-oriented semiactive suspensions.* Journal of dynamic systems, measurement, and control, 2005. **127**(2): p. 218-229.
31. Savaresi, S.M. and C. Spelta, *Mixed sky-hook and ADD: Approaching the filtering limits of a semi-active suspension.* Journal of dynamic systems, measurement, and control, 2007. **129**(4): p. 382-392.
32. Tang, J., Cao, D., Qin, Z., Li, H., & Chen, D. (2018). *A VCM-based novel whole-spacecraft vibration isolation device: simulation and experiment*. Journal of Vibroengineering, 20(2).
33. Zhang, Y. W., Fang, B., & Zang, J. (2015). *Dynamic features of passive whole-spacecraft vibration isolation platform based on non-probabilistic reliability*. Journal of Vibration and Control, 21(1), 60-67.
34. Zhang, Y., Zang, J., Fang, B., & Ji, S. (2014). *Dynamic characteristics of integrated active and passive whole-spacecraft vibration isolation platform based on non-probabilistic reliability.* Transactions of the Japan Society for Aeronautical and Space Sciences, 57(5), 263-271.